Journal of Materials Chemistry B

PAPER

Check for updates

Modular molecular design of polymerized pro-estrogen materials enables controlled astrocyte response†

Devan L. Puhl,‡[ab] Alexis Ziemba, (ID) ‡[ab] Samuel A. T. Ellman,‡[c] Alex Hsu,[c] Jayant Saksena,[abc] Penelope Phillips Falcone,[c] Bailey Balouch,[b] Deniz Rende,[d] Tanner Fink,[ae] R. Helen Zha, (ID) [ae] Ryan J. Gilbert*[ab] and Edmund F. Palermo (ID) *[abcd]

The hormone 17β-estradiol (estrogen or "E2") has demonstrated robust neuroprotective properties in countering oxidative stress-induced neurotoxicity, as well as strong neurotrophic properties to promote axonal growth, following injury to the central nervous system (CNS). However, oral or injected E2 is a suboptimal drug, as systemic administration fails to achieve a therapeutic dose at the injury site, in addition to being contraindicated in most male patients. Polymerized pro-drug biomaterials can mitigate these issues by locally releasing small quantities of drug over vastly extended timescales. We sought to study the effect of the biomaterial properties of poly(pro-E2) on astrocyte-surface interactions because astrocytes are the most abundant cell type in the central nervous system, play vital roles in neuron support and traumatic injury, and express estrogen receptors. Herein, we sought to study the effect of novel poly(pro-E2) films on astrocyte behavior, as well as to gauge the biomaterial properties that would lead to optimal astrocyte functionality. We synthesized pro-E2 as carbonate and ester derivatives and copolymerized each of these monomers with either oligoethylene glycol dithiol (EG) or hexylene dithiol (Hex) linkers to generate four unique poly(pro-E2) materials with tunable physiochemical and mechanical properties. We found that films of polymer with Hex-linkers supported sustained astrocyte adhesion, whereas the EG-linked analogs did not. To explain this behavior, we investigated the physical and chemical surface properties that may influence cell attachment. SEM images for films incubated in buffer showed marked surface roughness with micro- and nano-scale topography for the polymers with Hex-linkers, whereas those with EG-linkers appeared smooth. This result suggests that astrocytes preferentially adhere to rougher surfaces. Hex-linked polymer surfaces also demonstrated more negative zeta potentials compared to EG-linked polymer surfaces – indicating favorable electrostatic interactions for astrocyte adhesion. Finally, while all polymers exhibited hysteresis during mechanical testing, films with Hex-linkers demonstrated greater dissipation, suggesting more pronounced viscoelasticity. Taken together, these results indicate that a combination of physiochemical surfaces properties, which arise from subtle differences in chemical composition, can exert marked effects on astrocyte adhesion and spreading.

[a] Center for Biotechnology & Interdisciplinary Studies, Rensselaer Polytechnic Institute, 110 8th St., Troy, NY 12180, USA. E-mail: palere@rpi.edu, gilber2@rpi.edu

[b] Biomedical Engineering, Rensselaer Polytechnic Institute, 110 8th St., Troy, NY 12180, USA

[c] Materials Science & Engineering, Rensselaer Polytechnic Institute, 110 8th St., Troy, NY 12180, USA

[d] Center for Materials Devices & Integrated Systems, Rensselaer Polytechnic Institute, 110 8th St., Troy, NY 12180, USA

[e] Chemical & Biological Engineering, Rensselaer Polytechnic Institute, 110 8th St., Troy, NY 12180, USA

† Electronic supplementary information (ESI) available. See DOI: https://doi.org/10.1039/d5tb00285k

‡ These authors contributed equally to this work and share first authorship.

Introduction

There is an urgent need for interventions that can improve functional recovery and quality of life following traumatic injury to the central nervous system (CNS).[1] Astrocytes are a key cell type involved in the injury response; their role as a principal neuronal support cell shifts to leading a process known as astrogliosis.[2] Astrogliosis leads to the formation of the glial scar, which is prohibitive of neural regeneration, and is thus a critical target for nervous system injuries.[3] One way to target astrocytes and induce neuroprotective mechanisms is through exposure to the steroid hormone, 17β-estradiol ("estrogen" or "E2"). E2 has been shown

to be neuroprotective in nervous system injury and disease, and estrogen receptors (ER) are expressed on astrocytes.[4,5] ERα is highly expressed in astrocytes with nuclear localization,[6] with increased expression following injury.[7] Nanoparticles containing estrogen have shown promise in improving recovery from SCI in animal models.[8–10] Further, studies using a neuroautoimmune mouse model have shown that activation of ERα on astrocytes is neuroprotective.[11,12] However, systemic delivery of E2 fails to achieve therapeutic doses locally at the site of the lesions and causes adverse effects as a result of hepatic metabolism, in addition to being contraindicated in most male patients.[13,14] Further development of estrogen biomaterials that can locally deliver estrogen offers a solution to these challenges.

Prodrugs are chemically modified derivatives of drug molecules intended to improve their pharmacological performance. These prodrugs undergo chemical transformations *in vivo* to release the active parent drug, which then exerts the desired biological effect, typically over longer timescales.[15,16] Polymerized pro-drugs extend such small molecules into long chain macromolecules, in which every repeating unit in the polymer chain contains a pro-drug embedded in the structure.[17] The advantages of polymerized drugs include higher drug loading and longer-lasting release profiles relative to soluble small molecule prodrugs. Additionally, polyprodrugs can be processed into biomaterials with a wide variety of geometries and mechanical properties to serve as implantable depots of drug that will eventually fully resorb. Consequently, development of E2 prodrugs has generated considerable interest.[18–21] In this context, our laboratories have been interested in developing E2 polyprodrugs as biomaterials that modulate response to injuries of the central nervous system.[22–25] For spinal cord injury, the chronic progression of diseases proceeds on the timescale of many years, requiring much slower release rates than soluble small-molecule prodrugs can typically achieve. Moreover, local release at the site of the injury is desired to avoid off-target effects associated with systemic administration of E2. Hence, we sought to develop polymerized poly(pro-E2) thermoplastic materials capable of local implantation and slow degradation. In our previous work, we developed a polycarbonate alternating copolymer of E2 and oligoethylene glycol,

which showed neurotrophic and neuroprotective effects *in vitro*,[22] and promising preliminary neuroprotective effects *in vivo*.[26]

While our previous work on E2 polycarbonates demonstrated promise for modestly increasing neuron density at the lesion site, there remains a need to precisely tune the polyprodrug properties to minimize the inhibitory and toxic injury response of various CNS cell types following CNS injuries. The rate of E2 release from the polyprodrug scaffold is controlled primarily by the hydrolytic stability and the hydrophobicity. Hence, we postulated that the E2 release rate from this polymer can be precisely tuned by modifying the species E2 is copolymerized with and linkages between these species to provide a broad range of thermomechanical properties, degradation rates, and consequently modulated cell-biomaterial interactions. In this paper, we leveraged a modular molecular design platform to tailor the physiochemical attributes of polymerized E2-based materials. First, two pro-drugs of E2 were synthesized: homobifunctionalized with either allyl chloroformate to form the carbonate-linked bis-allyl species **1** (Fig. S1, ESI†) or with pentenoic acid to form the ester-linked bis-alkene **2** (Fig. S4, ESI†). Next, each of these prodrugs was then copolymerized with either 1,2-bis(2-mercaptoethoxy)ethane, a flexible dithiol based on an ethylene glycol unit, or 1,6-hexenedithiol, a somewhat less flexible but putatively more hydrophobic linker. Thus, we generated a series of four E2 polymers (Fig. 1). The four polymer types were then processed into films, characterized for their physical and thermomechanical material properties, tested for cytotoxicity with primary cortical cultures, and investigated for their influence on the behavior of primary cortical astrocytes.

Results and discussion

Monomer and polymer synthesis

Two hydrolytically labile pro-drugs of 17β-estradiol (E2), either as the carbonate (**1**) or ester (**2**) derivative bearing pendant alkenes, were copolymerized with either a dithiol linker (**3**) or a hydrophobic 1,6-hexylenedithiol (**4**) linker, *via* UV-photoinitiated thiol–ene radical addition chemistry in concentrated THF solution (Fig. S7, S10, S13 and S16, ESI†), following our previously published method[22] with minor modifications. Details of all
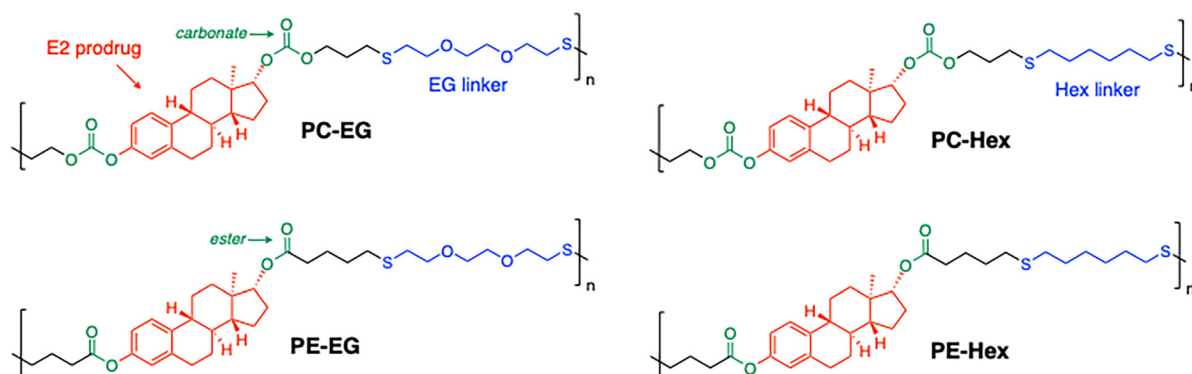

Fig. 1 Structure of poly(pro-E2) as polycarbonates or polyesters containing either EG or Hex type linker groups, in alternating sequence, prepared by photoinitiated thiol–ene radical addition.

This journal is © The Royal Society of Chemistry 2025

J. Mater. Chem. B, 2025, **13**, 6376–6392 | **6377**

synthetic procedures are given in the Methods section and characterization data are given in the ESI.† Owing to the step-growth nature of this polymerization, careful control of the stoichiometric equivalence was of paramount importance. This resulted in a library of poly(pro-E2) polymers: **PC-EG** *i.e.* poly(**1**-*alt*-**3**), **PC-Hex** *i.e.* poly(**1**-*alt*-**4**), **PE-EG** *i.e.* poly(**2**-*alt*-**3**), and **PE-Hex** *i.e.* poly(**2**-*alt*-**4**). The polymer structures are shown in Fig. 1.

Polymer characterization

Polymer structures were confirmed by NMR and are consistent with established precedent.[22] The ^{1}H and ^{13}C NMR spectra for each monomer and alternating copolymer are given in the ESI† (Fig. S8, S11, S14 and S17). It is clear from the resonances in the region of $\sim$5–6 ppm that the alkene groups of the monomer (**1** or **2**) are mostly consumed in the polymerization, consistent with a high degree of conversion, >95% in all cases. The molecular weight distributions (MWD) were estimated by GPC in THF at 40 °C, relative to polystyrene standards. We obtained four distinct alternating copolymers with comparable M_w in the range of 40–60 kDa and a peak molecular weight M_p in the range of 20–40 kDa. For all four samples, the MWDs span a broad range encompassing $\sim$10^3–10^5 g mol^{-1} with high dispersities (Đ $\sim$ 3–4), which is unsurprising due to the inherently stochastic nature of step-growth processes. Specific characterization data are summarized Table 1.

Thermal properties. Glass transition temperatures (T_g) were observed in all cases, whereas no evidence of a melting endotherm was observed, suggesting that all the samples are fully amorphous (Fig. 2B). The T_g values depend sensitively on both the type of degradable unit (ester *vs.* carbonate) as well as the linker unit (EG *vs.* Hex), since these subtle changes in chemical composition have a substantial impact on the restricted freedom of bond rotation and thus chain mobility. Polycarbonates yielded higher T_g in comparison to polyesters; and the Hex linkers yielded higher T_g than EG linker. The T_g of **PE-EG** ($\sim$3 °C) is lower than that of **PE-Hex** ($\sim$10 °C), and the T_g of **PC-EG** ($\sim$24 °C) is lower than that of **PC-Hex** ($\sim$44 °C). Both findings are consistent with the notion that a greater degree of chain mobility is associated with lower T_g. It is known that carbonate bonds are less polar than esters and promote more chain ordering, which renders the chains more rigid and thus have higher T_g,[27] which is consistent with findings here. Hence, through systematic modification of the flexible linker unit, the thermal properties can be tuned over a wide range. As a result, the mechanical properties, chemical properties, and degradation kinetics are influenced in turn, allowing for highly tailorable drug delivery system.

Hydrophobicity. Films of each polymer were prepared by drop casting from solution (5% in chloroform) onto glass
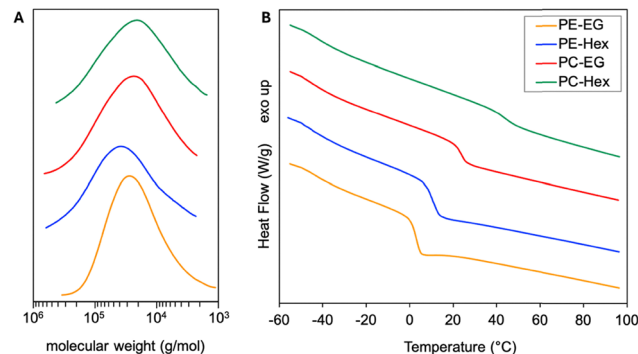

Fig. 2 Characterization of poly(pro-E2) materials. (A) Molecular weight distribution by gel permeation chromatography (GPC) and (B) thermal transitions quantified by differential scanning calorimetry (DSC).

slides, followed by solvent evaporation. The hydrophobicity of each material coating was investigated by contact angle goniometry. Static equilibrium water contact angles unfortunately could not be reached because the angles continuously decreased as a function of time and never plateaued to an equilibrium value within the time limit of droplet evaporation (Fig. S20, ESI†). All films showed a steady linear decrease in contact angle as time progressed. This is likely due to water penetration into the polymer and/or polymer chain dynamics at the water/polymer interface rearranging to minimize surface tension.[28] Surprisingly, across all of the time points we interrogated, the water contact angle on polymer films containing the Hex type linker ($\theta = 74°$ for **PE-Hex**, 78° for **PC-Hex**, at time 0) were lower than those containing EG type linkers ($\theta = 94°$ for **PE-EG**, 86° for **PC-EG**, at time 0). Intuitively, we had expected the opposite result because hexylene groups are more non-polar compared to ethylene glycol ethers. However, the kinetics of water spreading on or penetrating into the films may be more facile in the case of Hex linkers if there is a difference in surface roughness, which is indeed a complicating factor here (*vide infra*). Such kinetic differences might overshadow underlying differences in the equilibrium state that was inaccessible experimentally here.

Mechanical properties. We investigated the mechanical properties of these four E2-containing copolymers by nanoindentation of drop-cast films (Fig. 3). Those polymers containing Hex linkers displayed significantly greater elastic moduli compared to the EG-containing counterparts, which is in accord with expectations based on the lower T_g and greater chain flexibility of the EG-containing copolymers. Indeed, the average reduced elastic modulus for **PE-EG** ($E_r = 0.86$ GPa) and **PC-EG** (0.44 GPa) are much softer than those of **PE-Hex** (7.4 GPa) and **PC-Hex** (4.6 GPa), which is indeed the case with high significance ($p < 0.01$, Fig. 3). Among the copolymers with hexylene linkages, **PE-Hex** is significantly stiffer than **PC-Hex** ($p < 0.01$, Fig. 3E). The higher stiffness of Hex-linked polymers can be explained in part by the increased rotational freedom present in the ether bonds in the EG-linked polymers, compared to that of aliphatic carbon chains in Hex-linked polymers, since material stiffness is derived in part from the chain mobility in polymer systems.[29] The greater hardness of **PC-Hex** compared to the

Table 1 Summary of characterization data for polymerized estrogens in this work

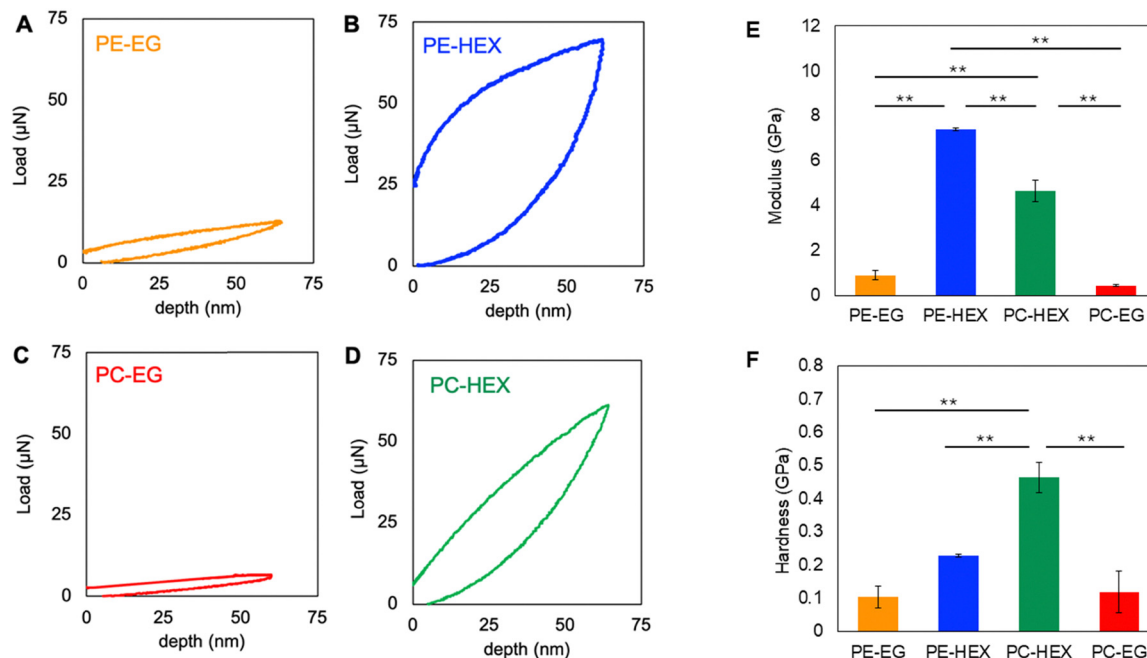| Polymer	M_p (kDa)	Đ	T_g (°C)	E (GPa)	θ ($t = 0$)
PE-EG	28.1	2.72	3	0.86	94°
PE-Hex	38.4	4.20	10	7.4	74°
PC-EG	21.0	3.34	24	0.44	86°
PC-Hex	24.1	4.03	44	4.6	78°

Fig. 3 Mechanical properties of poly(pro-E2) materials as drop-cast films characterized by nanoindentation. (A)–(D) Load displacement curves for poly(pro-E2) films. Hex-linked polymers displayed 7–8× more energy dissipation compared to EG-linked polymers. (E) and (F) Comparison of the Young's Modulus (E) and (F) stiffness of the poly(pro-E2) films. Significance was determined at $p = 0.05$; *$p < 0.05$, **$p < 0.01$.

other polymers could be explained based on the temperature of the experiment relative to the materials respective T_g values. As mentioned above, carbonate bonds are less flexible than esters and thus have higher T_g,[27] which is consistent with greater stiffness at room temperature. Nanoindentation data were collected at room temperature, and only **PC-Hex** is below its T_g at 25 °C whereas the other polymers are above their T_g (Fig. 2B). It is likely that **PC-Hex** will be somewhat softer at physiological temperatures nearer to its T_g ($\sim$44 °C).

Finally, nanoindentation data clearly indicate that while all polymers exhibited hysteresis during mechanical testing, Hex-linked polymers demonstrated greater energy dissipation, as indicated by the areas of their elastic hysteresis loops, with **PC-Hex** showing 7× and **PE-Hex** showing 8× greater energy dissipation compared to their counterparts, **PC-EG** and **PE-EG**, respectively, suggesting pronounced viscoelastic creep.[30] Viscoelasticity is generally a favorable material property for improved adhesion and function of cells, including astrocytes[31,32] and spinal tissue itself is notably viscoelastic in nature.[33]

Polymer film degradation

With the four representative polymers in hand, we proceeded to examine their degradation behavior as drop-cast films submerged in phosphate buffered saline (PBS) for extended periods of time (up to 6 weeks). Films were solution drop-cast onto glass slides, rigorously dried, and biopsy punched to 12 mm round disks. Disk dimensions and film thickness were finely controlled such that the surface:volume ratio and total initial mass were nearly identical across all four films. The films had an initial thickness of $\sim$100 µm and weighed $\sim$18 mg total starting mass. The as-cast films appear optically clear, colorless

and smooth in the initial dry state, to the naked eye. We monitored their erosion in terms of mass loss as a function of incubation time, changes in surface appearance by optical microscopy, changes in thickness by profilometry, and changes to the microscopic surface roughness by SEM. Finally, changes in the MWD were quantified by GPC on the remaining intact polymer films as well as methanolic extracts of any soluble intermediary degradation products (presumably including oligomers and small molecule pro-E2 fragments).

Mass loss. We quantified the mass loss from poly(pro-E2) disks incubated at 60 °C (accelerated degradation conditions) in PBS for over 6 weeks, to estimate the timescale over which the polymers degrade and release soluble components (E2 and pro-E2 fragments) into the surrounding media. Film mass loss was studied under accelerated conditions to produce quantifiable mass changes in an accessible time frame. After incubation for a specified time point, the films were removed from PBC, rinsed with deionized water to remove buffer salts, and were then rigorously dried to constant mass under vacuum. The mass loss data showed that **PE-Hex** degrades considerably faster than the other three polymers (Fig. 4). While this is consistent with the fact that polyesters often degrade faster than polycarbonates, it was initially unclear why **PE-Hex** demonstrated faster degradation than **PE-EG**, for example. Given their markedly different thermal and mechanical properties, it is possible that the explanation lies in the details of their erosion mechanism. Accordingly, we proceeded to further examine their surface appearance, thickness, and MWD as a function of degradation time.

Optical imaging. The as-cast films of all four polymers visually appeared clear and transparent upon evaporation of the casting solvent and drying overnight in vacuum to constant

This journal is © The Royal Society of Chemistry 2025

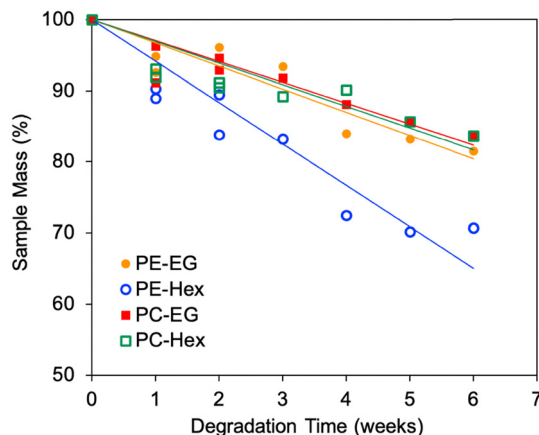*J. Mater. Chem. B*, 2025, **13**, 6376–6392 | **6379**

Fig. 4 Mass loss characterization of drop-cast poly(pro-E2) films at 60 °C in PBS.
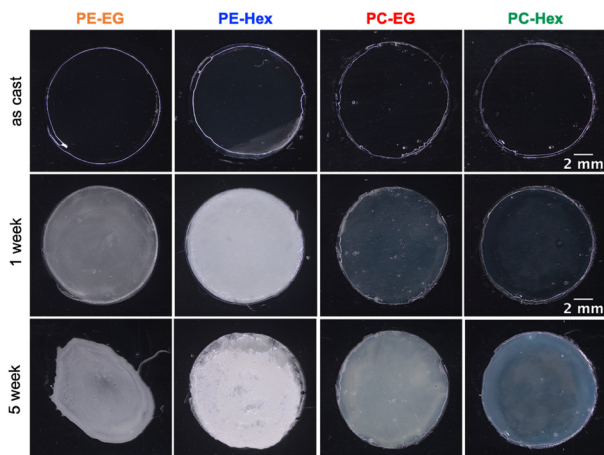

Fig. 5 Photos of poly(pro-E2) films incubated at 37 °C in PBS (in the wet state) for 1 and 5 weeks.

initial mass. Upon incubation at 37 °C for 1-week, visible changes in the optical properties of these films start to become evident to the naked eye (Fig. 5). For **PE-Hex** in particular, substantial turbidity develops with the first week of incubation and becomes even more pronounced after 5 weeks. At prolonged times, all four become cloudy, though to differing extents. Interestingly, **PE-EG** exhibits a shape distortion from its as-cast circular cross-section, suggesting this material flows as a very viscous fluid over 5 weeks at 37 °C. This result is reasonable given the T_g (3 °C) is much lower than the incubation temperature and non-crosslinked linear polymers are expected to have terminal flow behavior at temperatures much higher than T_g. The other three films, which all have higher T_g values, appeared not to distort substantially from their initial circular geometry. It is noteworthy that the turbidity of these films is seen in the wet state, but upon drying they return to a transparent appearance (Fig. S21, ESI†).

Profilometry. The thickness of the drop-cast films of each of the four polymers in this study were examined by profilometry (Fig. 6). Each of the as-cast samples have a smooth, flat surface of approximately 100 μm average thickness, except for **PC-Hex**, which appears mounded in the center up to about 170 μm maximum thickness in the center. This **PC-Hex** material has the highest T_g and is the hardest film mechanically, which possibly correlates with the mounding effect – perhaps due to higher solution viscosity on drying from organic solvent, slowing the spreading of the film to constant thickness under gravity. All four films are very close to the nominal diameter expected from using a 12-mm biopsy punch to fabricate them. Interestingly, **PE-Hex** appears to swell substantially and becomes wavy in surface texture on the mm scale. An increase in thickness, despite the observed mass loss (in the dry state), strongly indicate a mechanism of degradation that is largely dominated by bulk erosion rather than surface-limited erosion, especially for **PE-Hex** but less so for others. **PE-EG** appears to also swell, but preferentially around the outer rim of the circular film. **PC-EG** swells to a minor
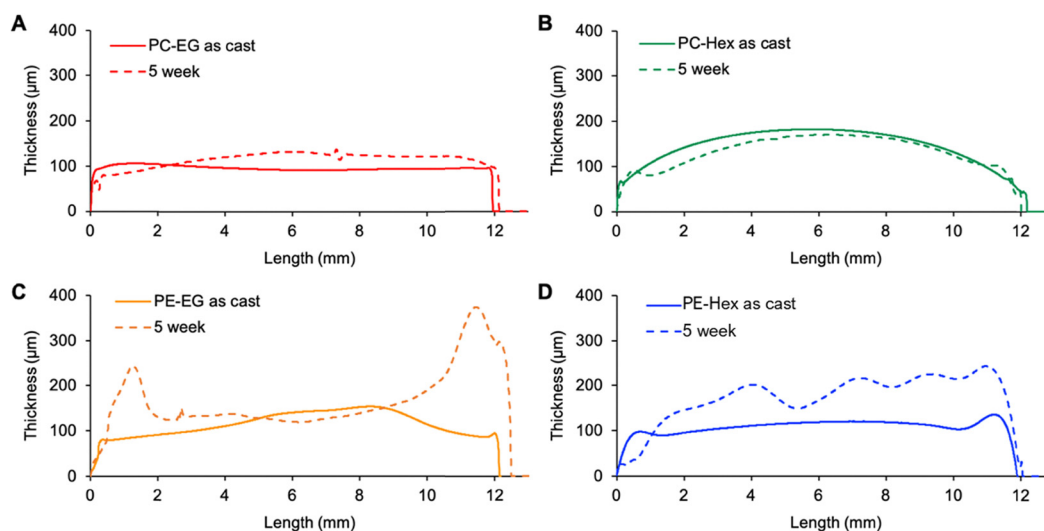

Fig. 6 Thickness of the poly(pro-E2) films: (A) **PC-EG**, (B) **PC-Hex**, (C) **PE-EG**, and (D) **PE-Hex** before and after incubation in PBS at 37 °C for 5 weeks.

6380 | J. Mater. Chem. B, 2025, **13**, 6376–6392

This journal is © The Royal Society of Chemistry 2025

extent, almost uniformly across the film. Only **PC-Hex** did not appear to swell and, if anything, slightly decreased in thickness. That result suggests **PC-Hex** may undergo surface erosion to some extent, which also seems to correlate with its relatively high T_g and high hardness by nanoindentation.

SEM images. The topography of the four as-cast films all appear smooth and featureless at $150\times$ magnification in the SEM (Fig. 7). After 1-week, **PE-Hex** begins to reveal "craters" of ~ 10–$20~\mu m$ diameter on the surface that were not present in the as-cast films. The other three samples show little obvious change at this 1-week timepoint. The simplest explanation for the crater effect is that drying of the wet films under vacuum requires water vapor to escape from within the material, leaving behind these circular features. In turn, that observation would suggest a bulk-erosion mechanism in which appreciable quantity of water penetrates deep into the bulk of these thick films. After 4 weeks, the difference in film appearance becomes even more pronounced. **PE-Hex** displays a preponderance of many craters, suggesting a more substantial efflux of water (and thus, a grater quantity of water embedded in the bulk). On the other hand, **PE-EG** appears to have partially delaminated from the glass substrate. This material has the lowest T_g and behaves like a viscous liquid at $37~^\circ C$. Thus, the hydrophobic material can flow slowly over 4 weeks to minimize contact area with the aqueous solution. This result supports the notion of surface-limited erosion for **PE-EG**, in contrast with bulk erosion for **PE-Hex**, and agrees with the counter-intuitive finding that **PE-EG** is more hydrophobic than **PE-Hex** in terms of water contact angle.

At still higher magnification in the SEM, microscopic roughness was revealed in the polymers containing Hex linkers, but not for those containing EG linkers (Fig. 8). The heterogenous erosion observed in Hex-linked polymers might be due to microscale phase separation that occurs upon partial hydrolysis of the polymer chains. Though initially these materials are indeed hydrophobic, ester or carbonate hydrolysis converts relatively non-polar linkages into more hydrophilic hydroxy, phenol and carboxylic acid moieties, which in turn admit further water penetration and thus could locally accelerate the hydrolysis process.

Acidic byproducts, in particular, have been shown to have an autocatalytic effect on degradation leading to significant decreases in MWD.[34,35] Local regions of hydrophilic material could then phase separate from intact, hydrophobic polymer, leading to the rough textured surfaces that are evident in the SEM micrographs for Hex-linked polymers, but not so for their EG-linked counterparts. For those polymers with a T_g well below $37~^\circ C$ (all but **PC-Hex**), we expect the phase separation to be facile. The increased roughness of **PE-Hex** could be attributed to greater phase separation between the hydrophilic and hydrophobic components of the polyester material.[36–40] Since **PC-Hex** is the harder, higher-T_g material, the polymer has limited mobility, and the spatial extent of phase segregation appears limited to the sub-micron length scale.

Molecular weight distribution. To further understand the degradation mechanisms of poly(pro-E2) films, as a function of their linker chemistry, we incubated films in PBS at $37~^\circ C$ for 6-weeks and measured their MWD by GPC, as compared to that of the initial polymer before degradation (Fig. 9A–D). After incubation, films were desalted by rinsing with deionized water and then dried before analysis by GPC in THF. In parallel, we also rinsed the polymers with methanol, which is known to be a non-solvent for the intact polymer, to extract out soluble small molecules and oligomers entrapped within the partially degraded films (Fig. 9E).
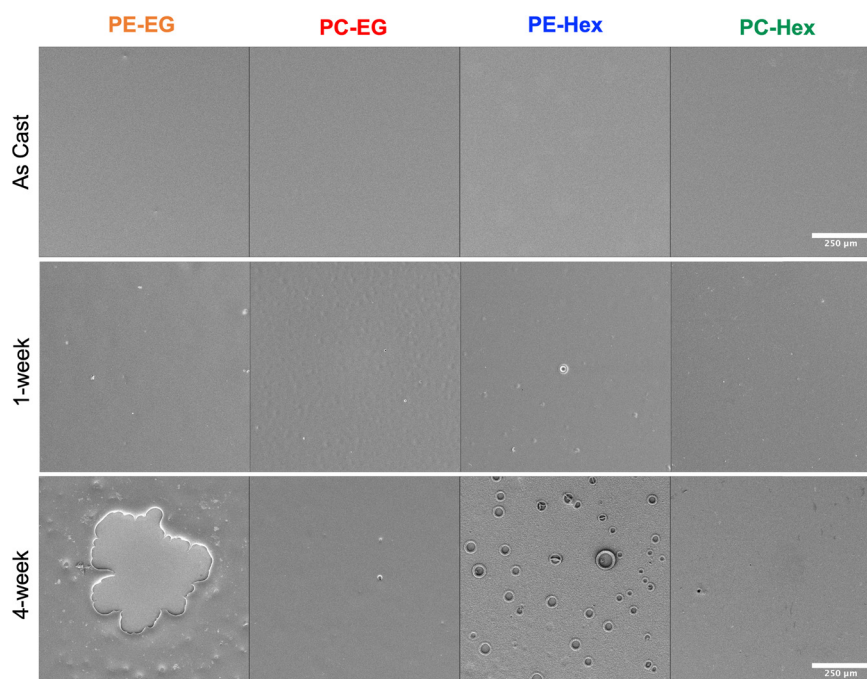

Fig. 7 SEM images of the four polymer films as-cast and after 1- and 4-weeks incubation ($37~^\circ C$, PBS). In all images, the scale bar is 250 μm.

This journal is © The Royal Society of Chemistry 2025

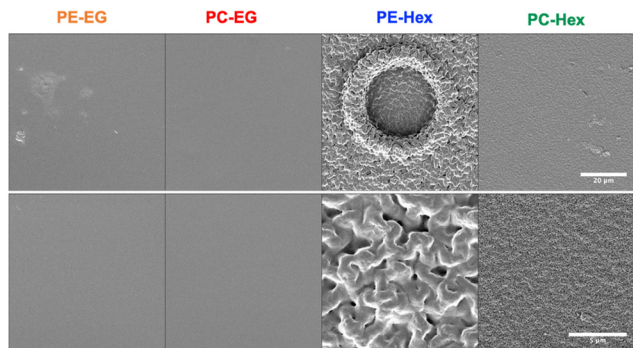*J. Mater. Chem. B*, 2025, **13**, 6376–6392 | **6381**

Fig. 8 Scanning electron microscopy images for surface characterization of submerged poly(pro-E2) films after 5-week incubation (37 °C, PBS) at two different magnifications. The scale bars are 20 μm for the upper row and 5 μm for the lower row.

The GPC traces of the MeOH-insoluble intact polymer films reveal some interesting trends. The hydrophobic polyester **PE-Hex**, which showed the most pronounced mass loss, also shows the most pronounced reduction in average molecular weight. After 6 weeks incubation at 37 °C in PBS, the entire MWD shifts to later elution time (smaller size) and new oligomeric peak grows in at about 14.2 min in the chromatograph. The M_w of **PE-Hex** is reduced by about 50% of its initial value. The hexylene-linked polyester **PE-EG**, on the other hand, shows a more modest shift in MWD to later elution times and the M_w drops to about 82% of its initial value. For the polycarbonates, marked differences are evident: the MWD of **PC-Hex** broadens only on the low-MW side while the high end remains relatively unchanged, resulting in a slight reduction of the average M_w value. In stark contrast, **PC-EG** appears to increase in MW due

to broadening on the high MW side of the distribution, to about 151% of its initial value. Combined with the knowledge that this polymer loses mass, the increase in average M_w of **PC-EG** could be due to selective cleavage of shorter chains near the surface, preferentially leaving behind the higher MW subpopulation. Other possibilities include aggregation in THF, crosslinking between chains during degradation, or perhaps oxidation of the thioethers to the sulfoxide or sulfone, expanding the hydrodynamic volume and thus GPC elution time, even in the absence of changes in chain length. Although the precise mechanism of crosslinking remains unknown at present, we suspect some crosslinking mechanism may be operative because a small subfraction of the MeOH-insoluble fraction was also THF-insoluble, leaving behind a trace quantity of THF-swollen, gel-like substance.

Considering that the **PC-EG** films did not appreciably swell, we speculate that **PC-EG** films of this ∼100 μm thickness may undergo surface-limited erosion. In our prior study on electrospun fibers (approximately 1 μm diameter) made from a different batch of the same material, we observed predominately bulk erosion at 80 °C.[22] The much thicker film geometry in this work appears to undergo surface erosion at 37 °C, on the other hand. Whereas both diffusion and hydrolysis kinetics are accelerated at higher temperature, greater thickness favors surface-limited erosion.[41]

Next, we examined the GPC traces of the methanolic extracts. Intact polymer is not methanol soluble, but short oligomers and small molecules that did not dissolve into the PBS may be extracted from the intact polymer in this manner. All four extracts show the same result: a multimodal distribution at late elution times corresponding to a MW in the range of ∼500–2000 g mol^{-1} (relative to PS standards). These are presumably short oligomers
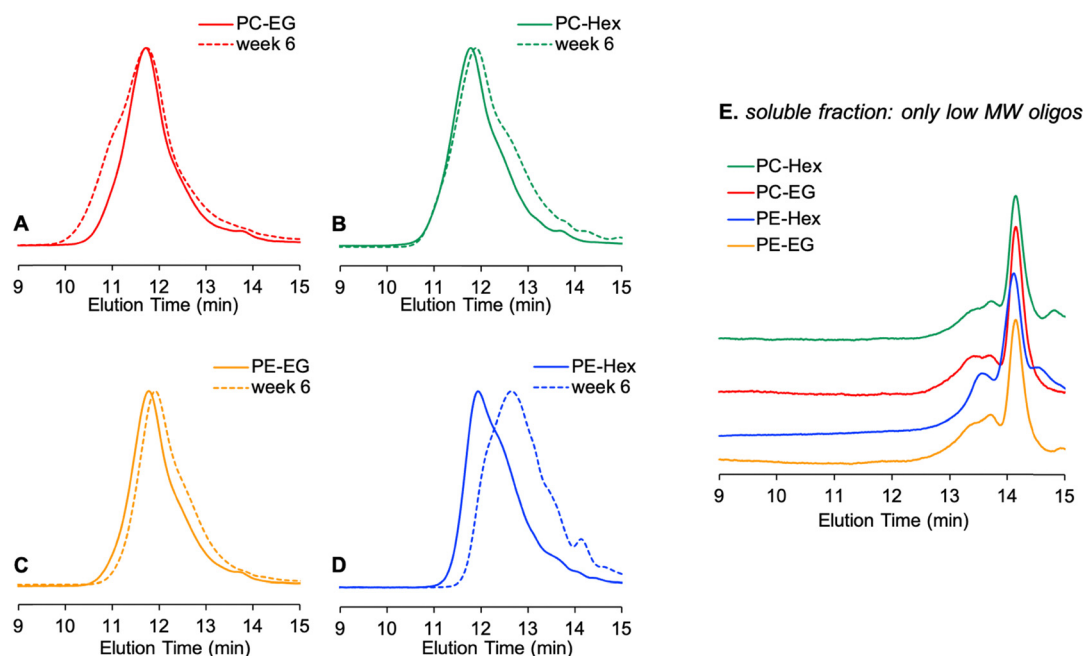

Fig. 9 Changes in the MWD for films of poly(pro-E2) incubated at 37 °C. (A)–(D) Methanol-insoluble films; (E) methanol-soluble fraction extracted from the remaining intact films.

6382 | J. Mater. Chem. B, 2025, **13**, 6376–6392

This journal is © The Royal Society of Chemistry 2025

or pro-drugs of E2 containing one or two pendant linkers which are MeOH-soluble but not readily released into PBS buffer. When pure E2 in THF is evaluated by GPC for comparison, a peak appears at ∼17 minutes, which is outside the calibration range for our PS standards. All the polymer samples displayed some feature in this region as well, but it is obscured by a much larger negative RI peak which may be related to residual salt carryover from the PBS. Therefore, some amount of pure E2 is retained within the remaining intact films and does not get released immediately into PBS buffer, presumably due to limited aqueous solubility of E2 and hydrophobic interactions between E2 and the remaining poly(pro-E2) films. We speculate that at much later degradation times, when little solid polymer remains, such residues would eventually get resorbed. Transport of cleaved drug from remaining polymer film into the surrounding media encompasses both the desorption of E2 or pro-E2 from the intact polymer film and then diffusion *via* percolation pathways to escape into free aqueous solution. While autocatalytic degradation mechanisms such as ester hydrolysis can accelerate degradation locally, size- and solubility-dependent drug transport may also strongly influence drug release kinetics.[34] Note, however, that these are incubations were done under static conditions *in vitro*. The release of soluble fragments from films *in vivo* would be less prone to such retention issues, where fluid flow and clearance are constantly at play. Therefore, we predict that release of soluble drug would occur faster in the case of dynamic clearance, all else being equal.

Cell-biomaterial interactions

Biocompatibility. To determine whether the synthesized polyestrogens produce any toxic byproducts, primary rat mixed cortical cells were cultured for 7 days with the poly(pro-E2) polymer films. Cell viability was assessed *via* two methods: (1) the percentage of propidium iodide (PI)-stained (dead) cells was compared to the percentage of Hoechst-stained (total) cells

and (2) the level of lactate dehydrogenase (LDH) in the supernatant for each group was quantified and normalized to the LDH signal for an entire lysed well (Fig. 10 and 11). No significant toxic effect adversely affecting cell viability compared to control (no treatment) was observed with any polymer or with soluble E2. During PI staining, all groups showed 3% or fewer total cells dead with no significant differences between the treatment and control groups ($F_{6,14} = 1.05$, $p = 0.438$). The LDH assay showed 14% or fewer cells dead with no significant differences between the treatment and control groups ($F_{6,14} = 0.58$, $p = 0.739$). While the polyesters resulted in slightly higher cell death compared to control, the difference was not statistically significant. A possible explanation could be certain byproducts from polyester hydrolysis that are toxic to cortical cells; for example, Kim *et al.* observed that aromatic degradation products, such as styrene glycol, were more toxic to HeLa cells.[42]
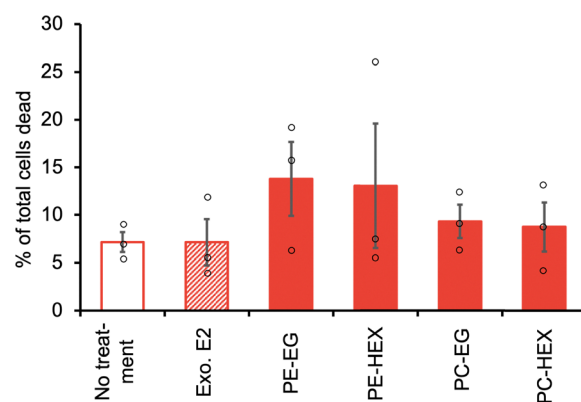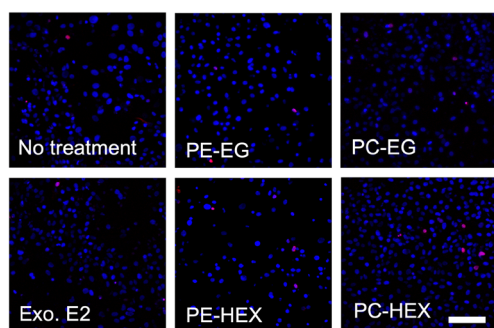

Fig. 11 Poly(pro-E2) materials did not significantly affect the viability of cortical cells *in vitro*. Percentage of total percentage of dead cells using LDH assay after 7-day exposure (data are not significantly different by one-way ANOVA). Measurements were done in triplicate and the error bars represent average ± standard deviation. None of the polymer groups are statistically different from no treatment: $F[5,12] = 0.67$, $p = 0.652$ (one-way ANOVA).
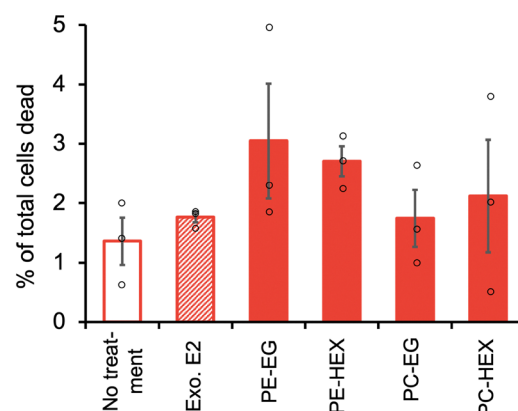

Fig. 10 Poly(pro-E2) materials did not significantly affect the viability of cortical cells *in vitro*. (A) PI-stained dead cells (red) after 7-day exposure (scale bar = 100 μm) compared to the total number of cells stained by Hoechst (blue). (B) Summary graph of % of total number of nonviable cells. Measurements were done in triplicate and the error bars represent average ± standard deviation. None of the polymer groups are statistically different from no treatment: $F[5,12] = 1.07$, $p = 0.422$ (one-way ANOVA).

This journal is © The Royal Society of Chemistry 2025

*J. Mater. Chem. B*, 2025, **13**, 6376–6392 | **6383**

Astrocyte adhesion and spreading. Astrocytes are the most abundant cell type in the central nervous system (CNS) and are responsible for maintaining homeostasis. Astrocyte function is quite complex and the significance of adhesion and spreading to a surface varies based on the intended application. For example, in instances of CNS tissue loss and grafting, it would be beneficial for astrocytes to infiltrate and adhere to synthetic or biologically-derived scaffolds to support neurite outgrowth through the scaffold and formation and maturation of synapses. As astrocytes play a major role at the blood–brain barrier and in angiogenesis, their adhesion will be critical for the vascularization of the scaffolding that supports neurons.[43] In CNS injury and disease, astrocytes take on a reactive phenotype where the astrocytes form a barrier that separates nervous system tissue from a fibrotic scar that aims to protect the nervous system tissue; this is includes astrocyte morphological changes that could be induced by introduction of a synthetic polymer surface.

In order to probe these effects, we cultured astrocytes on various polymer surfaces for 1 and 7 days, and then assessed the ability of cells to adhere and spread on the surfaces. As controls for comparison, we have included astrocytes on bare glass alone (see ESI†), glass coated with a garden-variety polyester containing no drug (**PLLA** films), as well as **PLLA** films with exogenous E2 added to the culture media. Astrocytes hardly adhere to bare glass (negative control) but they stick well to **PLLA** coatings (positive control). This comparison shows the effect of switching from a hard inorganic surface to a softer polymer material in the absence of drug. The samples that have PLLA + exogenous E2 show the role of free estrogen, if any, on the adhesion events; this simulates what would be the case for a partially degraded polyestrogen that has released some free E2 into the surrounding media.

Because astrocytes express ERα and are key targets to mediate neuroprotective activity,[5,7,11,12] primary rat cortical astrocytes were cultured directly onto each polymer substrate for 1 day or 7 days, and cell adhesion and spreading were assessed at each time point (Fig. 12 and 13, Table 2, Tables S3 and S4, ESI†). Although both the **PE-EG** and **PC-EG** films were not cytotoxic to mixed cortical cultures, astrocyte adhesion was
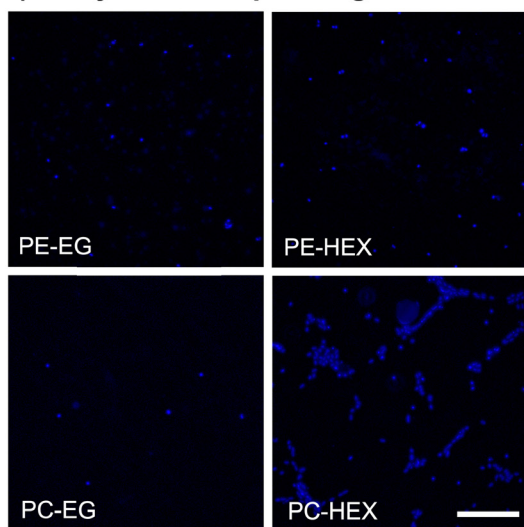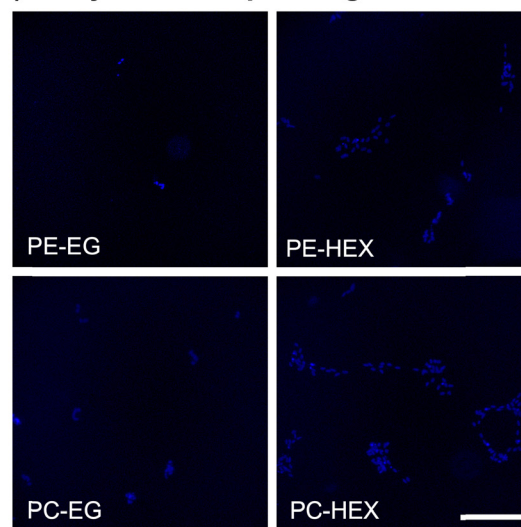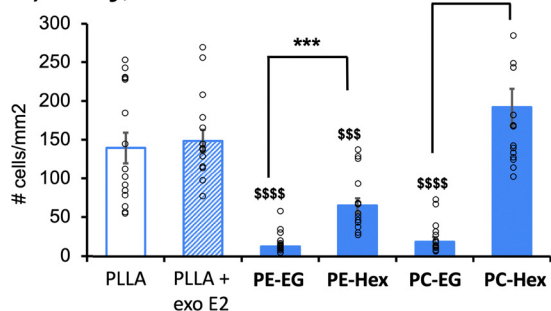

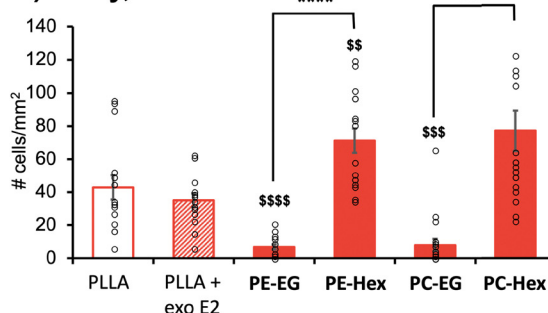**Fig. 12** Hex linkers support improved astrocyte adhesion. Astrocytes stained with DAPI after (A) 1 & (C) 7 days cultured on films (scale bar = 200 μm). Number of astrocytes adhered per mm^2 after (B) 1 & (D) 7 days in culture. Statistical significance was determined using a Welch's ANOVA with Games-Howell *post hoc* test. The symbol $ denotes a significant difference between **PLLA + Exo. E2** and all other groups. The symbol * denotes a significant difference of **PE-EG** *vs.* **PE-Hex** or between **PC-EG** and **PC-Hex**. The symbols denote confidence as \$,* $p \leq 0.05$, \$\$,** $p \leq 0.01$, \$\$,*** $p \leq 0.001$, and \$\$,**** $p \leq 0.0001$.

6384 | *J. Mater. Chem. B*, 2025, **13**, 6376–6392

This journal is © The Royal Society of Chemistry 2025
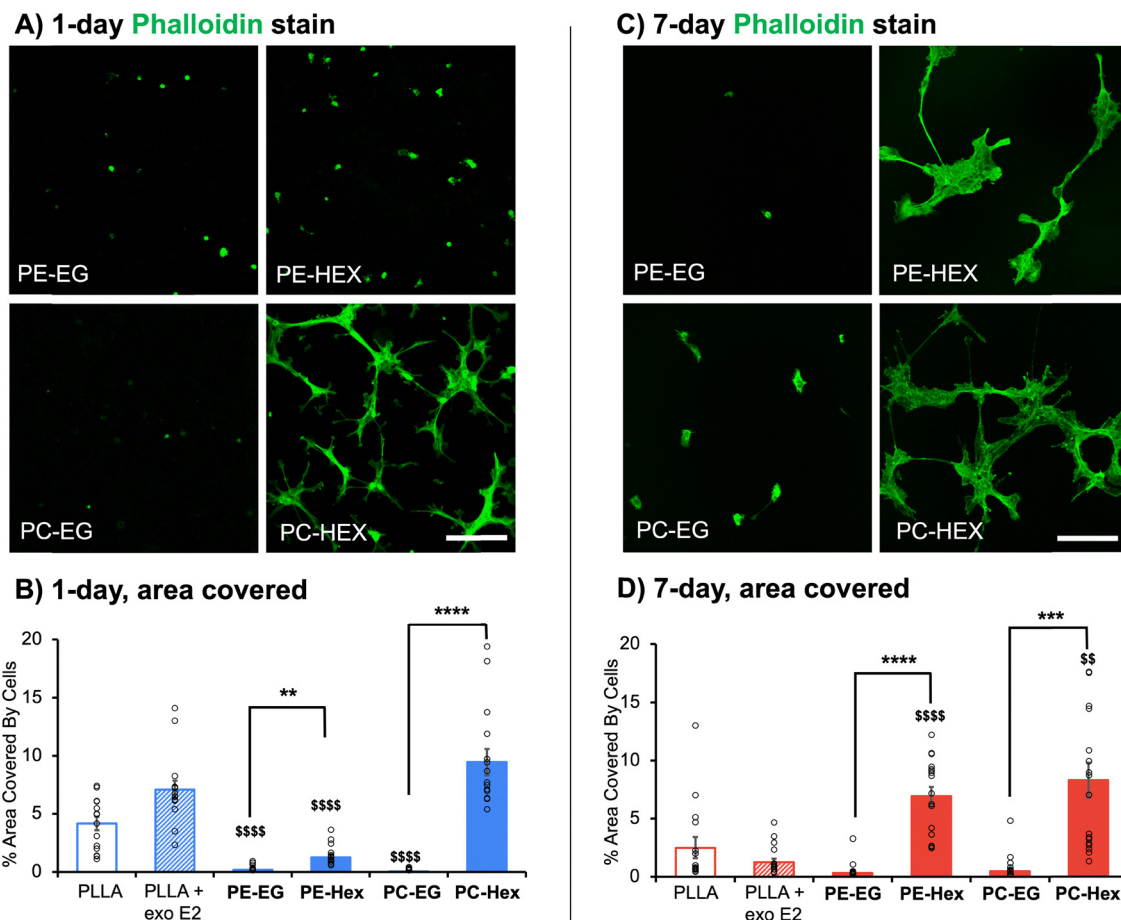
Fig. 13 Hexyl linkers support improved astrocyte spreading. Astrocytes stained with phalloidin after (A) 1 & (C) 7 days cultured on films (scale bar = 200 μm). Percentage of total area covered by astrocytes adhered per mm^2 after (B) 1 & (D) 7 days in culture. Statistical significance was determined using a Welch's ANOVA with Games–Howell *post hoc* test. The symbol \$ denotes a significant difference between **PLLA + Exo. E2** and all other groups. The symbol * denotes a significant difference of **PE-EG** *vs.* **PE-Hex** or between **PC-EG** and **PC-Hex**. The symbols denote confidence as \$,* $p \leq 0.05$; \$\$,** $p \leq 0.01$, \$\$;*** $p \leq 0.001$; and \$\$,**** $p \leq 0.0001$.

Table 2 Astrocyte adhesion and spreading on films

Material	Adhesion (cells per mm^2)		Spreading (% surface area covered)	
	1 day	7 day	1 day	7 day
PLLA + Exo. E2	149.52 ± 14.31	34.93 ± 4.20	7.09 ± 0.78	1.25 ± 0.31
PE-EG	12.72 ± 3.63	6.89 ± 1.56	0.18 ± 0.06	0.33 ± 0.19
PE-HEX	65.47 ± 9.39	71.35 ± 7.30	1.26 ± 0.23	6.93 ± 0.80
PC-EG	18.98 ± 5.47	8.00 ± 3.63	0.04 ± 0.02	0.47 ± 0.25
PC-HEX	192.65 ± 23.92	77.00 ± 12.30	9.46 ± 1.13	8.29 ± 1.50

significantly reduced on EG-linked polymer films. Both the **PE-Hex** and **PC-Hex** films showed significantly greater cell adhesion compared to their EG-linked counterparts following both 1 day ($F_{7,47.10} = 32.83$; PE: $p \leq 0.001$; PC: $p \leq 0.0001$) and 7 days ($F_{7,51.46} = 20.08$; PE: $p \leq 0.0001$; PC: $p \leq 0.001$) in culture directly on the surface of untreated polymer films (Fig. 12). Additionally, both the **PE-Hex** and **PC-Hex** films showed significantly greater cell spreading compared to their EG-linked counterparts following both 1 day ($F_{7,43.53} = 45.24$; PE: $p \leq 0.01$; PC: $p \leq 0.0001$) and 7 days ($F_{7,50.55} = 14.28$; PE:

$p \leq 0.0001$; PC: $p \leq 0.001$) in culture directly on the surface of untreated polymer films (Fig. 13). **PE-EG** and **PC-EG** also showed reduced cell adhesion compared to the **PLLA + Exo. E2** control at both 1 day ($F_{7,47.10} = 32.83$; PE: $p \leq 0.0001$; PC: $p \leq 0.0001$) and 7 days ($F_{7,51.46} = 20.08$; PE: $p \leq 0.0001$; PC: $p \leq 0.001$). However, **PE-EG** and **PC-EG** only showed a significant reduction in cell spreading compared to the **PLLA + Exo. E2** control at 1 day ($F_{7,43.53} = 45.24$; PE: $p \leq 0.0001$; PC: $p \leq 0.0001$). By 7 days, cell spreading on both **PE-EG** and **PC-EG** was comparable to the **PLLA + Exo. E2** control. This

indicates that although the **PLLA + Exo. E2** control supported improved initial adhesion and spreading compared to both EG-containing substrates, it did not support spreading long-term in serum-free media conditions. However, the Hex-containing films resulted in superior astrocyte adhesion and spreading long-term compared to the **PLLA + Exo. E2** control. **PE-Hex** films initially showed reduced cell adhesion ($F_{7,47.10} = 32.83$, $p \leq 0.001$) and spreading ($F_{7,43.53} = 45.24$, $p \leq 0.0001$) compared with the **PLLA + Exo. E2** control at 1 day; however, **PE-Hex** showed significantly greater cell adhesion ($F_{7,51.46} = 20.08$, $p \leq 0.01$) and spreading ($F_{7,50.55} = 14.28$, $p \leq 0.0001$) compared with the **PLLA + Exo. E2** control at 7 days. **PC-Hex** showed similar levels of cell adhesion compared to the **PLLA + Exo. E2** control at both 1-day and 7-day time points. **PC-Hex** also showed similar levels of cell spreading compared with the **PLLA + Exo. E2** control at 1 day; however, **PC-Hex** supported significantly greater cell spreading compared with the **PLLA + Exo. E2** control at 7 days ($F_{7,50.55} = 14.28$, $p \leq 0.01$).

The reduced cell adhesion and spreading that was observed on both the **PE-EG** and **PC-EG** compared to the Hex-containing polymers and **PLLA + Exo. E2** control may be due to repulsive interactions between the cellular membrane and the EG linkers. Astrocytes have a highly negative resting membrane potential.[44] Such potential arises from accumulation of negatively-charged ions on the intracellular side of the membrane and positively-charged ions on the extracellular side of the membrane.[45] The electronegative oxygen atoms within ethylene glycol linkages in the polymer chains are also known to attract positively-charged ions in solution.[46–48] The association of cations in medium surrounding the astrocytes with EG is thought to, in part, lead to repulsive interactions between the astrocytes and the EG-containing polymers, ultimately reducing cell adhesion to EG-containing substrates.[48] To investigate the interaction of ions in solution with the polymer films, we conducted zeta potential measurements on each of the polymer groups (Fig. 14). The results indeed show that both the **PE-EG** and **PC-EG** have significantly less negative zeta potentials (-46.87 ± 11.68 and -58.44 ± 10.32 mV, respectively) compared to their Hex-linked counterparts (**PE-Hex:** -61.02 ± 11.74 mV; **PC-Hex:** -92.65 ± 4.13 mV) ($F_{4,40} = 32.31$; PE: $p \leq 0.01$; PC: $p \leq 0.0001$). The **PE-EG** group also showed a less negative zeta potential compared to the **PLLA** control (-67.10 ± 2.23 mV) ($F_{4,40} = 32.31$; PE: $p \leq 0.001$). Additionally, **PC-Hex** showed a significantly more negative zeta potential compared to the **PLLA** control ($F_{4,40} = 32.31$; PE: $p \leq 0.0001$). In summary, the trends in zeta potential reflect the trends observed in the initial astrocyte adhesion and spreading data; the collection of a greater number of cations at the surface of the substrates, most notably at the surface of the EG-containing poly(pro-E2) materials, potentially contributes to increased repulsion of astrocytes with negative membrane potentials that have attracted cations around the cell surface.

Because only the textured polymerized estrogen films in this work showed markedly higher adhesion and spreading, compared to PLLA + exogenous E2 controls, it is clear that specific some characteristics of the Hex type materials must be mediating their interactions with astrocytes at the interface. The
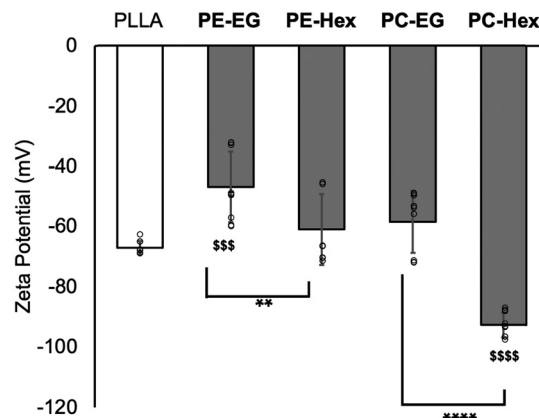

Fig. 14 Poly(pro-E2) materials containing EG linkers attract a greater number of positively charged ions to their surface compared to those containing Hex linkers. Zeta potential of each film using a 10 mM pH 7.4 solution. All data are represented by the mean zeta potential $\pm$ the standard deviation and overlayed with points representing individual replicates for each group. Significance was determined by one-way ANOVA. The symbol $\$$ denotes a significant difference between **PLLA + Exo. E2** and all other groups. The symbol * denotes a significant difference of **PE-EG** vs. **PE-Hex** or between **PC-EG** vs. **PC-Hex**. The symbols denote confidence according to: $\$$ or * $p \leq 0.05$; $\$\$$ or ** $p \leq 0.01$; $\$\$$ or *** $p \leq 0.001$; and $\$\$$ or **** $p \leq 0.0001$.

improved astrocyte interactions with the **PE-Hex** and **PC-Hex** substrates over the longer-term may be due to the combination of less cationic surface charge and increased surface roughness over time. Images of the poly(pro-E2) films show that the films initially appear smooth and transparent; however, upon 1 week of incubation in PBS at 37 °C, the **PE-Hex** and **PC-Hex** films become turbid. Based on SEM images of the film surfaces, we observed the formation of microscopic roughness on the surface of the **PE-Hex** and **PC-Hex** substrates. On the other hand, **PE-EG** and **PC-EG** remained locally smooth on the micro-scale throughout the 5-week incubation period, despite heterogeneities on longer $\sim$ mm length scales. Surface roughness caused by nanoscale topographical features is shown to positively influence cell adhesion and spreading.[49–52] For example, Ganguly et al. showed that nanoporous anodic aluminum oxide surfaces significantly improved rat cortical astrocyte adhesion compared to the nonporous aluminum control. In part, this effect may be due to the increased formation of focal adhesion sights on the nanoporous substrate compared to the smooth control.[52] Focal adhesion sites are formed through the mechanical linkage of cell transmembrane integrin proteins and extracellular ligands, and it is well established that an increase in these sites leads to increase cell adhesion strength and cell spreading.[53,54]

Further, free thiols are known to bond with integrins on the cell surface to improve the formation of cell adhesion sites and, in turn, improve cell adhesion and spreading.[55–57] Since all of the poly(pro-E2) materials were synthesized with dithiol type linkers, it was expected that these polymers would likely contain some amount of unreacted free thiols at the chain ends. Thus, we investigated whether a difference in concentration of free thiols could contribute to the changes in cell adhesion and spreading observed on the different substrates (Fig. S19, ESI†).

6386 | J. Mater. Chem. B, 2025, **13**, 6376–6392

This journal is © The Royal Society of Chemistry 2025

Using Ellman's test, all polyestrogens were found to have a significantly greater concentration of free thiols (**PE-EG:** 51.02 ± 1.05 nM; **PE-Hex:** 46.61 ± 1.22 nM; **PC-EG:** 52.43 ± 0.49 nM; **PC-Hex:** 47.18 ± 3.10 nM) compared to the **PLLA** control that should have no thiols (26.37 ± 0.47 nM) ($F_{5,12}$ = 160.00; $p \leq 0.0001$ for all). We also observed a significantly greater concentration of free thiols in the **PE-EG** and **PC-EG** substrates compared to their Hex-linked counterparts ($F_{5,12}$ = 160.00; PE: $p \leq 0.05$; PC: $p \leq 0.01$). This observation could be due to the increased ability of aqueous solutions to penetrate within the ethylene glycol-containing substrates compared to those containing hexyl linkers, resulting in a greater number of reactions between the Ellman's reagent and free thiols to occur. Although these observations do not strictly indicate interactions at the film surface, the short incubation time of 15 minutes likely precludes contributions from deep within the bulk. Given that the EG-linked polymers showed markedly lower astrocyte adhesion/spreading, despite containing slightly higher free thiol content, we reject the notion that the presence of free thiols in the polyestrogen films substantially impacts the astrocyte adhesion and spreading.

Finally, it has been demonstrated that viscoelastic microenvironments that lead to favorable biomechanical properties in astrocytes for promoting neural regeneration in the CNS under inflammatory conditions.[30–32,58] Since the Hex-linked polymers exhibit the greatest degree of hysteresis and surface roughness compared to other polymer analogues in this work, this may also contribute to astrocyte longer-term adhesion and spreading on Hex-linked polymers.

Conclusions

Estrogen is known for its neurotrophic and neuroprotective actions, and estrogen variants have been studied extensively for the treatment of stroke, Alzheimer's, Parkinson's, and CNS injury.[59] Astrocytes are a promising target for estrogen therapeutics due to their expression of ERα, which has been shown to mediate neuroprotective activity. Previous studies by our group found poly(pro-E2) films to be neuroprotective against oxidative stress and to enhance neurite outgrowth of dorsal root ganglia neurons *in vitro*,[22] which suggested that polymerized forms of estrogen can maintain estrogen bioactivity and could be particularly beneficial for CNS injuries that require localized treatment over an extended period (months to years).

In this work, we developed a series of poly(pro-E2) films with tunable thermal and mechanical properties and demonstrate a range of different erosion mechanisms *in vitro*. This work provides an innovative and tunable synthetic approach to yield poly(pro-estrogens) biomaterials with varying linkers and degradable units, reveals how linker chemistry in polyprodrugs influences thermal/mechanical properties, degradability, and surface properties, and demonstrates poly(pro-drug) materials with the ability to promote specific astrocyte behaviors. Interestingly, we found that increased micro/nano-scale surface roughness and more negative zeta potential, as well as increased mechanical

hysteresis, appear to correlate with robust astrocyte adhesion and spreading. Owing to their lack of cytotoxicity and ability to modulate astrocyte response, our novel library of tunable poly(pro-E2) polymers can be utilized to target CNS injuries and disorders more effectively. For future *in vivo* and clinical translation of our novel poly(pro-E2) slow-eluting materials, we anticipate that the films, which encourage astrocyte adhesion and spreading, would be ideal for applications involving placement of scaffolds or conduits to encourage nerve regrowth, while those poly(pro-E2) materials that discourage astrocyte adhesion and spreading *i.e.*, the EG-linked polymers, would be useful as coatings for stents or shunts (to drain excess fluid), structural implants and microelectrodes, to record neural activity or deliver electrical stimulation to assist with nerve regrowth but resist cell attachment.

Materials and methods

Synthesis and characterization

Polymerized estrogen materials were prepared following our previously described route with minor modifications. All detailed procedures are given in the ESI.† The ^{1}H and ^{13}C NMR are given in the ESI.† Spectra were recorded using 500 MHz Agilent NMR spectrometer at 25 °C. NMR chemical shifts were reported in parts per million (ppm, δ) and referenced to tetramethylsilane ($(CH_3)_4Si$, 0.00 ppm). Residual solvent signals for ^{1}H NMR: CDCl$_3$ (δ 7.26), DMSO-d6 (δ 2.50) and ^{13}C NMR: CDCl$_3$ (δ 77.0), DMSO-d6 (δ 39.5).

Gel permeation chromatography (GPC) performed on an Agilent Technologies 1260 Infinity GPC with THF as the mobile phase (100 µL injection volume, 1 mL min^{-1} flow rate). Polymer MW was then determined using monodisperse polystyrene standards. High resolution mass spectroscopy (HRMS) was performed on Thermo LTQ Orbitrap XL instrument at resolution 30 000 (at m/z 400) and mass accuracy better than 3 ppm. Samples were injected in the ESI† source using Agilent 1200 HPLC system in methanol as a mobile phase at flow rate 50 µl min^{-1}.

Polymer film casting. All polymer groups were mixed on a stir plate with chloroform to create a 5% (w/w polymer/chloroform) solution. Once homogenous, a 50 µL volume of each 5% film solution was drop-cast onto 15 mm × 15 mm glass coverslips, and the films were placed under high vacuum overnight to remove residual solvent. Films were then frozen at −80 °C and circular disks were obtained using a 12-mm biopsy punch.

Degradation. To characterize degradation kinetics of poly(pro-E2) variants, 4 films (∼18 mg polymer per film), prepared by solution drop-casting were analyzed. Prior to analysis, films were cooled to below their respective glass transition temperature (T_g), biopsy punched to 12 mm circular disk and peeled off the glass slides to maintain uniform surface area. Films were then transferred to 20 mL scintillation vials and weighed on an analytical balance with a resolution of 0.00001 g. Films were submerged in 20 mL of PBS (0.1 M, pH 7.4) and incubated under accelerated conditions at 60 °C due to the increased mass and slow degradation rates. Every week, one sample was removed for analysis. PBS was collected, then replaced with 20 mL of fresh PBS for the remaining samples

This journal is © The Royal Society of Chemistry 2025

J. Mater. Chem. B, 2025, **13**, 6376–6392 | **6387**

to maintain sink conditions. At each timepoint, PBS solutions were stored at −20 °C until quantification of E2 concentrations. For the sample under analysis, films were rinsed with 10 mL of millQ water to remove residual salt which was subsequently added to the corresponding PBS sample. Following the milli Q rinse, 10 mL of methanol was added, and the polymer was soaked for 1 h. The sample was then divided into a methanol soluble and methanol insoluble fraction. Methanol was removed by rotary evaporation and vacuum dried to constant mass (48 h, 30 mTorr). The fraction was then weighed on an analytical balance with a resolution of ±0.00001 g. The fraction was then taken for GPC analysis to observe changes in the MWD and the presence of E2. The methanol insoluble fraction was vacuum dried till constant mass (48 h, 30 mTorr). The fraction was then weighed and taken for GPC analysis to observe changes in the MWD over time.

Contact angle goniometry. Contact angle was measured using a DSA 100 goniometer. A 10 μL droplet of water was transferred onto the polymer film and video recorded over the course of 10 minutes. The test was run in duplicate, at two different positions per film.

Thermal properties. Relevant thermal transition temperatures of the poly(pro-E2) were characterized using differential scanning calorimetry (DSC). Thermal analysis was conducted using a DSC-Q2000 (TA Instruments). The instrument was calibrated against an indium standard. The samples (3–8 mg) were hermetically sealed into aluminum sample pans (TA Instruments). Empty pans were used as a reference. The samples were subjected to a heat/cool/heat cycle to erase previous thermal history. The samples were first equilibrated to −70 °C then heated at a rate of 10 °C min^{-1} from −70 °C to 250 °C, cooled at a rate of 5 °C min^{-1} to −70 °C, and heated at a rate of 10 °C min^{-1} to 250 °C under N$_2$ flow (40.00 mL min^{-1}).

Mechanical properties. Nanoindentation experiments were performed with a Hysitron TriboIndenter (Hysitron Inc., Minneapolis, MN) in a load-controlled instrument with a load resolution of 100 nN, displacement resolution of 1 nm, and maximum indentation depth of 5 μm. For all experiments, a Berkovich tip with radius of 100 nm (TI-0039, Hysitron) was used. A series of nanoindentation measurements were performed on fused silica standard (S/N 5-0098, Hysitron) to calculate the contact area function parameters, as instructed by the manufacturer. Before nanoindentation experiments, the fused silica was tested to assure the standard modulus and hardness values are $E_r = 69.9 \pm 5\%$ and $H = 9.1$ GPa $\pm 10\%$. The experiments were performed at room temperature on polymers drop-cast on glass slides. To eliminate any substrate effects (Chan, *et al.*, 2000), the displacement-controlled load function (60 nm) with 12 nm s^{-1} loading and unloading times was used. Only **PC-EG** sample was tested with 1 nm s^{-1} loading and unloading rate to achieve better control to approach sample. Each sample was tested using an automated run at least 25 indents at multiple positions, and one representative curve was presented for comparison. The reduced modulus (E_r) was calculated from curve fitting to the unloading segment. The elastic modulus (E) was then calculated through the relationship:

$$\frac{1}{E_r} = \frac{\left(1 - v_i^2\right)}{E_i} + \frac{\left(1 - v_s^2\right)}{E_s} \quad (1)$$

where v_i and v_s are the Poisson's ratio of the diamond Berkovich indenter (0.07) and sample (0.3), respectively, and E_i is the modulus of the indenter (1140 GPa) as provided by the manufacturer.[60,61] The energy dissipated during elastic hysteresis was calculated by taking the difference between the areas under the load displacement curves.[30]

Cell assays

Mixed cortical culture. The following procedure was approved by the Rensselaer Polytechnic Institute Institutional Animal Care and Use Committee. P2 Sprague Dawley rat pups were euthanized by rapid decapitation. Brains were extracted, and the meninges were removed. The olfactory bulb, cerebellum, midbrain, and hippocampus were removed, and the cortex was stored in OptiMEM on ice until dissociation. Brains from two animals were combined and considered to be one biological replicate. The cortex was chopped into smaller pieces using a size 15 scalpel blade. The tissue was then rinsed with Hank's balanced salt solution (HBSS) (5 mL) and spun down at 100 rcf for 5 min. HBSS was decanted and TrypLE Express (5 mL) was added to the chopped tissue. The tissue was incubated at 37 °C/5% CO$_2$ for 20 min with flicking every 5 min to ensure enzymatic degradation of the tissue. After 20 min, horse serum (5 mL) was added, and the solution was triturated to quench the trypsin. The tissue was spun down at 100 rcf for 5 min. The supernatant was decanted and replaced with Dulbecco's modified Eagle medium (DMEM) + 10% fetal bovine serum (FBS), 10% F-12 nutrient supplement, and 1% penicillin–streptomycin (PS). Using a 16-gauge needle and 5 mL syringe, the tissue was triturated 10 times and then filtered through a 100-μm filter to remove large chunks of tissue. Cells were then counted, confirming the number of viable cells using Trypan Blue and a hemocytometer. Cells were plated onto poly-L-lysine-coated coverslips at a density of 200 000 cells/78.5-mm^2 coverslip in DMEM + 10% FBS, 10% F-12 nutrient supplement, and 1% PS. After 24 h at 37 °C/5% CO$_2$, cells were rinsed once with HBSS then media was replaced with neurobasal medium + L-glutamine (200 mM), B-27 (2%), and PS (1%) for 12 days. On day 13, media was replaced with 2.25 mL of media to fully submerge a 15 × 15 mm coverslip with drop cast polymer. Cell incubation conditions were as follows: media only (no treatment), media + exogenous E2 (Exo. E2) (100 nM), **PE-EG** film, **PE-Hex** film, **PC-EG** film, and **PC-Hex** film. Cells were incubated with the polymers for 7 days at which point the supernatant was collected to conduct a lactate dehydrogenase (LDH) assay, and the cells were stained with propidium iodide (PI) and Hoechst 33342 for imaging ($n = 3$ biological replicates from different animals).

Live/dead imaging assay. To visualize the percentage of dead cells in response to each condition, after a 7-day incubation, the cells were first washed with imaging solution (10 mM HEPES, pH 7.4, containing 140 mM NaCl, 5 mM KCl, 2 mM CaCl$_2$, 2 mM MgCl$_2$, 5 mM D-glucose) and then incubated with Hoechst 33342 trihydrochloride trihydrate (10 μg mL^{-1} in imaging solution) and propidium iodide (PI) (2 μg mL^{-1} in imaging solution) with Pluronic F-127 (0.25% w/v in DMSO). Following this incubation, the cells were washed 3 times with

6388 | *J. Mater. Chem. B*, 2025, **13**, 6376–6392

This journal is © The Royal Society of Chemistry 2025

imaging solution, and the viability markers were visualized using an Olympus IX-81 confocal microscope. Five fields of view on coverslips from each biological replicate ($n = 3$) were imaged using $20\times$ magnification. The number of propidium iodide-positive cells and Hoechst-positive cells were counted, and the ratio was taken to assess the percent of cells dead. The mean percentages of dead cells for each biological replicate were averaged. Data were represented as the mean percent of total cells dead ± standard error of the mean.

Lactate dehydrogenase assay. After a 7-day incubation with various estrogen films, the supernatant was collected to assess levels of lactate dehydrogenase, which is indicative of cell death. The assay was conducted following the manufacturer's instructions. Briefly, the absorbance at 450 nm was taken for each well using a Tecan M200 plate reader. The NBM-only absorbance wells were subtracted from all other groups. All data were normalized to the absorbance of a completely lysed well (100% dead). Data were represented as the mean percent of total cells dead ± standard error of the mean with $n = 3$ biological replicates.

Cortical astrocyte culture. Cortical astrocytes were harvested from the same P2 Sprague Dawley rat pups abiding the same procedures. Brains from two animals were combined and considered to be one biological replicate. Cortex was chopped into smaller pieces using a size 15 scalpel blade. TrypLE (5 mL) and DNase I (1 mL at 1 mg mL^{-1}) were added to the chopped tissue. The tissue was incubated at 37 °C/5% CO$_2$ for 30 min with agitation every 7–8 min to dissociate the tissue. After 30 min, DMEM + 10% FBS, and 1% PS was added to quench enzymatic degradation. The tissue was spun down at 500 rcf for 5 min. The supernatant was decanted and replaced with DMEM + 10% FBS, and 1% PS and then seeded into T25 flasks. Cortical astrocytes were cultured for 13 days in DMEM + 10% FBS + 1% PS at 37 °C/5% CO$_2$ with regular media changes. On day 13, the T25 flasks were shaken at 180 rpm for 6 h and then washed with HBSS to remove non-astrocytic cell types. The cells were then washed with phenol red-free TrypLE and incubated in phenol red-free TrypLE (3 mL) for 10 min with tapping every 3 min. Cells were lifted and plated at 100 000 cells per 225 mm^2 coverslips and cultured for 1 day or 7 days in serum-free DMEM + 1% glutamax + 1% PS containing no phenol red or FBS; a 2.25 mL volume/12-well plate well was used to avoid media changes during the incubation periods. Astrocytes were cultured directly on the following substrates: glass coverslip only (glass), glass coverslip + Exo. E2 (100 nM), poly-L-lactic acid film (**PLLA**), **PLLA + Exo. E2** (100 nM), **PE-EG, PE-Hex, PC-EG**, and **PC-Hex**. Following the 1 day or 7 days culture, the cells were fixed and stained to assess astrocyte adhesion and spreading ($n = 3$ biological replicates from different animals).

Astrocyte adhesion and spreading. To assess cortical astrocyte adhesion and spreading following direct culture on each substrate, astrocytes were fixed for 12 min using paraformaldehyde (4% in PBS) and washed $3\times$ with PBS. After washing, astrocytes were blocked for nonspecific antibody binding and permeabilized by incubating in 5% bovine serum albumin (BSA) and 0.1% Tween-20 in PBS for 1 hour at room temperature. The culture was then probed for glial fibrillary acidic

protein (GFAP) by incubating with polyclonal rabbit anti-GFAP primary antibody (1 : 1000), diluted in 0.5% BSA and 0.1% Tween-20 in PBS overnight at 4 °C. Following three washes with 0.1% Tween-20 in PBS to remove residual primary antibody, cells were incubated with Alexa Fluor 594 goat anti-rabbit secondary antibody (1 : 1000) to label GFAP and Alexa Fluor 488 phalloidin (1 : 1000) to label f-actin in 0.5% BSA and 0.1% Tween-20 in PBS for 2 hours at room temperature. Nuclei were then counterstained by incubating with DAPI (1 : 1000) in PBS for 10 minutes. Cells were washed 3 times with PBS and then stored in PBS at 4 °C until imaged.

Cells were imaged using an Olympus IX-81 confocal microscope with a $10\times$ objective (five fields of view per $n = 3$ biological replicate coverslips), and maximum intensity projections were obtained from the z-stacks. DAPI-stained nuclei were counted using the ImageJ multi-point tool to quantify cell adhesion, and the phalloidin-stained images were analyzed with the automated thresholding ImageJ plugin to quantify the percent area covered by astrocytes in each $10\times$ field of view. Astrocyte adhesion data are represented as the mean number of cells per mm^2 ± standard error of the mean and astrocyte spreading data are represented by the mean percent area covered by cells ± standard error of the mean ($n = 3$ biological replicates for both cell adhesion and spreading).

Zeta potential. A 450 μL volume of each 5% (w/w polymer/chloroform) film solution was drop cast evenly across 25 mm × 75 mm micro slides and dried under high vacuum overnight. The material groups that were assessed are as follows: **PLLA, PE-EG, PE-Hex, PC-EG**, and **PC-Hex**. The zeta potential of each film was measured using an Anton Paar SurPASS 3 Electrokinetic Analyzer for solid surface analysis to determine the surface charge of each polymer. Each experiment was run using a 10 mM KCl solution at approximately physiological pH (7.61 ± 0.30). Once the conditions were equilibrated, 3 measurements were taken for each run and 3 separate runs were performed for each polymer type ($n = 3$ with 9 total measurements for all film groups).

Quantification of free thiols. A 50 μL volume of each 5% (w/w polymer/chloroform) film solution was dropast onto 15 mm × 15 mm glass coverslips as described previously, and the films were placed under high vacuum overnight to remove residual solvent. The material groups that were assessed are as follows: glass, **PLLA, PE-EG, PE-Hex, PC-EG**, and **PC-Hex**. Free thiols were quantified via an Ellman's assay. First, the reaction buffer (0.1 M sodium phosphate, pH 8.0, containing 1 mM EDTA) was prepared. Next, Ellman's reagent (5,5′-dithio-bis-(2-nitrobenzoic acid)) was dissolved in the reaction buffer at a concentration of 4 mg mL^{-1}. A standard curve was prepared by dissolving cysteine hydrochloride monohydrate in the reaction buffer at concentrations ranging from 0 mM–1.5 mM. The reaction solution was created by adding a 10 μL volume of 4 mg mL^{-1} Ellman's reagent solution to 500 μL of reaction buffer. Finally, 50 μL of each standard was added to its respective reaction solution and the 510 μL reaction solution was added onto each of the 50 μL drop cast polymer films or glass coverslip controls. Each reaction was protected from light

This journal is © The Royal Society of Chemistry 2025

J. Mater. Chem. B, 2025, **13**, 6376–6392 | **6389**

and incubated for 15 min. After 15 min, 200 μL of each standard and film reaction was added to a 96 well plate in duplicate and the absorbance at 412 nm was taken for each well using a Tecan M200 plate reader. The duplicate readings were averaged, and the 0 mM absorbance value was subtracted from each group. Each film group was plotted against the standard curve (r^2 = 0.999) to determine the concentration of free thiols in each polymer. The data were represented by the average concentration $\pm$ the standard deviation (n = 3 material replicates).

Statistical analyses. Minitab 19 was used for statistical analyses. All data for toxicity tests, astrocyte adhesion, astrocyte spreading, zeta potential, and Ellman's test were first assessed for normality using the Ryan-Joiner test and tested for equal variances. All toxicity, zeta potential, and Ellman's data were assessed using a one-way ANOVA with *post hoc* Tukey's test with $\alpha \leq 0.05$. All astrocyte adhesion and spreading data were assessed using a Welch's ANOVA with Games-Howell *post hoc* test with $\alpha \leq 0.05$. Complete statistical information for toxicity, astrocyte adhesion, astrocyte spreading, and Ellman's test assessments are reported in the ESI.†

Data availability

All raw data files were uploaded to Open Science Framework and can be accessed publicly at the following link: Palermo, E. F. (2025, February 7). Polyestrogen Astrocyte paper. Retrieved from osf.io/ybsw2.

Conflicts of interest

S. A. T. E., E. F. P. and R. J. G. are co-inventors on US Patent #11,202,834 which pertains to the polymerized estrogen chemistry used in this manuscript. The patent was filed on October 16, 2019.

Acknowledgements

References

1 C. S. Ahuja, J. R. Wilson, S. Nori, M. R. N. Kotter, C. Druschel, A. Curt and M. G. Fehlings, Traumatic Spinal Cord Injury, *Nat. Rev. Dis. Primers*, 2017, **3**(1), 1–21, DOI: 10.1038/nrdp.2017.18.

2 A. R. Filous and J. Silver, Targeting Astrocytes in CNS Injury and Disease: A Translational Research Approach, *Prog. Neurobiol.*, 2016, **144**, 173–187, DOI: 10.1016/j.pneurobio.2016.03.009.

3 S. Y. Ng and A. Y. W. Lee, Traumatic Brain Injuries: Pathophysiology and Potential Therapeutic Targets, *Front. Cell. Neurosci.*, 2019, **13**, 528, DOI: 10.3389/FNCEL.2019.00528.

4 K. M. Dhandapani and D. W. Brann, Role of Astrocytes in Estrogen-Mediated Neuroprotection, *Exp. Gerontol.*, 2007, **42**(1–2), 70–75, DOI: 10.1016/J.EXGER.2006.06.032.

5 E. Acaz-Fonseca, R. Sanchez-Gonzalez, I. Azcoitia, M. A. Arevalo and L. M. Garcia-Segura, Role of Astrocytes in the Neuroprotective Actions of 17β-Estradiol and Selective Estrogen Receptor Modulators, *Mol. Cell. Endocrinol.*, 2014, **389**(1–2), 48–57, DOI: 10.1016/J.MCE.2014.01.009.

6 D. Kata, I. Gróf, Z. Hoyk, E. Ducza, M. A. Deli, I. Zupkó and I. Földesi, Immunofluorescent Evidence for Nuclear Localization of Aromatase in Astrocytes in the Rat Central Nervous System, *Int. J. Mol. Sci.*, 2022, **23**(16), 8946, DOI: 10.3390/IJMS23168946/S1.

7 D. García-Ovejero, S. Veiga, L. M. García-Segura and L. L. Doncarlos, Glial Expression of Estrogen and Androgen Receptors after Rat Brain Injury, *J. Comp. Neurol.*, 2002, **450**(3), 256–271, DOI: 10.1002/CNE.10325.

8 A. Cox, M. Capone, D. Matzelle, A. Vertegel, M. Bredikhin, A. Varma, A. Haque, D. C. Shields and N. L. Banik, Nanoparticle-Based Estrogen Delivery to Spinal Cord Injury Site Reduces Local Parenchymal Destruction and Improves Functional Recovery, *J. Neurotrauma*, 2021, **38**(3), 342–352, DOI: 10.1089/NEU.2020.7047.

9 S. Samantaray, E. A. Sribnick, A. Das, N. P. Thakore, D. Matzelle, S. P. Yu, S. K. Ray, L. Wei and N. L. Banik, Neuroprotective Efficacy of Estrogen in Experimental Spinal Cord Injury in Rats, *Ann. N. Y. Acad. Sci.*, 2010, **1199**, 90–94, DOI: 10.1111/J.1749-6632.2009.05357.X.

10 E. A. Sribnick, J. M. Wingrave, D. D. Matzelle, S. K. Ray and N. L. Banik, Estrogen as a Neuroprotective Agent in the Treatment of Spinal Cord Injury, *Ann. N. Y. Acad. Sci.*, 2003, **993**, 125–133, DOI: 10.1111/J.1749-6632.2003.TB07521.X.

11 R. D. Spence, M. E. Hamby, E. Umeda, N. Itoh, S. Du, A. J. Wisdom, Y. Cao, G. Bondar, J. Lama, Y. Ao, F. Sandoval, S. Suriany, M. V. Sofroniew and R. R. Voskuhl, Neuroprotection Mediated through Estrogen Receptor-α in Astrocytes, *Proc. Natl. Acad. Sci. U. S. A.*, 2011, **108**(21), 8867–8872, DOI: 10.1073/PNAS.1103833108/SUPPL_FILE/PNAS.201103833SI.PDF.

12 R. D. Spence, A. J. Wisdom, Y. Cao, H. M. Hill, C. R. L. Mongerson, B. Stapornkul, N. Itoh, M. V. Sofroniew and R. R. Voskuhl, Estrogen Mediates Neuroprotection and Anti-Inflammatory Effects during EAE through ERα Signaling on Astrocytes But Not through ERβ Signaling on Astrocytes or Neurons, *J. Neurosci.*, 2013, **33**(26), 10924–10933, DOI: 10.1523/JNEUROSCI.0886-13.2013.

13 P. E. Ludwig, A. A. Patil, A. J. Chamczuk and D. K. Agrawal, Hormonal Therapy in Traumatic Spinal Cord Injury, *Am. J. Transl. Res.*, 2017, **9**(9), 3881–3895.

14 A. Coyoy-Salgado, J. Segura-Uribe, H. Salgado-Ceballos, T. Castillo-Mendieta, S. Sánchez-Torres, X. Freyermuth-Trujillo, C. Orozco-Barrios, S. Orozco-Suarez, I. Feria-Romero, R. Pinto-Almazán, G. Moralí de la Brena and C. Guerra-Araiza, Evaluating Sex Steroid Hormone Neuroprotection in Spinal Cord Injury in Animal Models: Is It Promising in the Clinic?, *Biomedicines*, 2024, **12**(7), 1478, DOI: 10.3390/biomedicines12071478.

15 M. Markovic, S. Ben-Shabat and A. Dahan, Prodrugs for Improved Drug Delivery: Lessons Learned from Recently Developed and Marketed Products, *Pharmaceutics*, 2020, **12**(11), 1–12, DOI: 10.3390/pharmaceutics12111031.

16 J. Rautio, N. A. Meanwell, L. Di and M. J. Hageman, The Expanding Role of Prodrugs in Contemporary Drug Design

6390 | *J. Mater. Chem. B*, 2025, **13**, 6376–6392

This journal is © The Royal Society of Chemistry 2025

and Development, *Nat. Rev. Drug Discovery*, 2018, **17**(8), 559–587, DOI: **10.1038/nrd.2018.46**.

17 F. Seidi, Y. Zhong, H. Xiao, Y. Jin and D. Crespy, Degradable Polyprodrugs: Design and Therapeutic Efficiency, *Chem. Soc. Rev.*, 2022, **51**(15), 6652–6703, DOI: **10.1039/d2cs00099g**.

18 W. Elger, R. Wyrwa, G. Ahmed, F. Meece, H. B. Nair, B. Santhamma, Z. Kileen, B. Schneider, R. Meister, H. Schubert, H. Schubert and K. Nickisch, Estradiol Prodrugs (EP) for Efficient Oral Estrogen Treatment and Abolished Effects on Estrogen Modulated Liver Functions, *J. Steroid Biochem. Mol. Biol.*, 2017, **165**, 305–311, DOI: **10.1016/j.jsbmb.2016.07.008**.

19 L. Prokai, V. Nguyen, S. Szarka, P. Garg, G. Sabnis, H. A. Bimonte-Nelson, K. J. McLaughlin, J. S. Talboom, C. D. Conrad, P. J. Shughrue, P. Koulen and K. Prokai-Tatrai, The Prodrug DHED Selectively Delivers 17β-Estradiol to the Brain for Treating Estrogen-Responsive Disorders, *Sci. Transl. Med.*, 2015, **7**(297), 297ra113, DOI: **10.1126/scitranslmed.aab1290**.

20 J. A. Pollock and H. K. Parker, Advances in the Development of Prodrugs as Selective Modulators of Estrogen Receptors, *J. Endocr. Soc.*, 2022, **6**(12), bvac158, DOI: **10.1210/jendso/bvac158**.

21 A. E. Salinero, C. Abi-Ghanem, H. Venkataganesh, A. Sura, R. M. Smith, C. A. Thrasher, R. D. Kelly, K. M. Hatcher, V. NyBlom, V. Shamlian, D. G. Zuloaga and K. L. Zuloaga, Treatment with Brain Specific Estrogen Prodrug Ameliorates Cognitive Effects of Surgical Menopause in Mice, *Horm. Behav.*, 2024, **164**, DOI: **10.1016/j.yhbeh.2024.105594**.

22 A. R. D'Amato, D. L. Puhl, S. A. T. Ellman, B. Balouch, R. J. Gilbert and E. F. Palermo, Vastly Extended Drug Release from Poly(pro-17β-Estradiol) Materials Facilitates in Vitro Neurotrophism and Neuroprotection, *Nat. Commun.*, 2019, **10**, 4830, DOI: **10.1038/s41467-019-12835-w**.

23 A. M. Ziemba and R. J. Gilbert, Biomaterials for Local, Controlled Drug Delivery to the Injured Spinal Cord, *Front. Pharmacol.*, 2017, **8**, 245, DOI: **10.3389/FPHAR.2017.00245/BIBTEX**.

24 A. M. Ziemba, M. C. C. Woodson, J. L. Funnell, D. Wich, B. Balouch, D. Rende, D. N. Amato, J. Bao, I. Oprea, D. Cao, E. F. Palermo and R. J. Gilbert, Development of a Slow-Degrading Polymerized Curcumin Coating for Intracortical Microelectrodes, *ACS Appl. Bio Mater.*, 2023, **6**(2), 806–818, DOI: **10.1021/acsabm.2c00969**.

25 R. Chen, J. Funnell, G. Quinones, M. Bentley, J. Capadona, R. Gilbert and E. Palermo, Poly(pro-Curcumin) Materials Exhibit Dual Release Rates and Prolonged Antioxidant Activity as Thin Films and Self-Assembled Particles, *Biomacromolecules*, 2022, **24**(1), 294–307, DOI: **10.1021/acs.biomac.2c01135**.

26 M. K. Gottipati, S. A. T. Ellman, D. L. Puhl, Z. Guan, P. G. Popovich, E. F. Palermo and R. J. Gilbert, Acute Dose-Dependent Neuroprotective Effects of Poly(pro-17β-Estradiol) in a Mouse Model of Spinal Contusion Injury, *ACS Chem. Neurosci.*, 2021, **12**(6), 959–965, DOI: **10.1021/acschemneuro.0c00798**.

27 F. Andriani and T. Fuoco, Statistical Enchainment of Ester/Ether and Carbonate Cleavable Bonds to Control Copolymers' Erosion Rate and Trigger Environment-Specific

Degradation, *Eur. Polym. J.*, 2022, **178**, 111457, DOI: **10.1016/J.EURPOLYMJ.2022.111457**.

28 X. Wang, Z. Chen and Z. Shen, Dynamic Behavior of Polymer Surface and the Time Dependence of Contact Angle, *Sci. China, Ser. B:Chem.*, 2005, **48**(6), 553–559, DOI: **10.1360/042004-22**.

29 J. Diani and P. Gilormini, Molecular Mobility with Respect to Accessible Volume in Monte Carlo Lattice Model for Polymers, *Phys. A*, 2017, **468**, 825–831, DOI: **10.1016/j.physa.2016.11.088**.

30 Y. Li and M. Xu, Hysteresis Loop and Energy Dissipation of Viscoelastic Solid Models, *Mech. Time-Depend. Mater.*, 2007, **11**(1), 1–14, DOI: **10.1007/s11043-007-9027-4**.

31 J. G. Roth, M. S. Huang, R. S. Navarro, J. T. Akram, B. L. LeSavage and S. C. Heilshorn, Tunable Hydrogel Viscoelasticity Modulates Human Neural Maturation, *Sci. Adv.*, 2023, **9**, eadh8313, DOI: **10.1126/SCIADV.ADH8313**.

32 Y.-B. Lu, K. Franze, G. Seifert, C. Steinhäuser, F. Kirchhoff, H. Wolburg, J. Guck, P. Janmey, E.-Q. Wei, J. Käs, J. Käs and A. Reichenbach, Viscoelastic Properties of Individual Glial Cells and Neurons in the CNS, *Proc. Natl. Acad. Sci. U. S. A.*, 2006, **103**(47), 17759–17764, DOI: **10.1073/pnas.0606150103**.

33 O. Neumann, H. V. Surana, S. Melly, P. Steinmann and S. Budday, Mechanical Characteristics of Spinal Cord Tissue by Indentation, *J. Mech. Behav. Biomed. Mater.*, 2025, **163**, 106863, DOI: **10.1016/J.JMBBM.2024.106863**.

34 L. N. Woodard and M. A. Grunlan, Hydrolytic Degradation and Erosion of Polyester Biomaterials, *ACS Macro Lett.*, 2018, **7**(8), 976–982, DOI: **10.1021/acsmacrolett.8b00424**.

35 H.-M. Chang, C.-C. Huang, V. R. Parasuraman, J.-J. Jhu, C.-Y. Tsai, H.-Y. Chao, Y.-L. Lee and H.-C. Tsai, In Vivo Degradation of Poly (ε-Caprolactone) Films in Gastro Intestinal (GI) Tract, *Mater. Today Commun.*, 2017, **11**, 18–25, DOI: **10.1016/j.mtcomm.2017.01.006**.

36 S. K. Saha and H. Tsuji, Effects of Molecular Weight and Small Amounts of D-Lactide Units on Hydrolytic Degradation of Poly(l-Lactic Acid)s, *Polym. Degrad. Stab.*, 2006, **91**(8), 1665–1673, DOI: **10.1016/j.polymdegradstab.2005.12.009**.

37 H. Tsuji, A. Mizuno and Y. Ikada, Properties and Morphology of Poly(L-Lactide). III. Effects of Initial Crystallinity on Long-Term in Vitro Hydrolysis of High Molecular Weight Poly(L-Lactide) Film in Phosphate-Buffered Solution, *J. Appl. Polym. Sci.*, 2000, **77**(7), 1452–1464, DOI: **10.1002/1097-4628(20000815)77:7<1452::AID-APP7>3.0.CO;2-S**.

38 R. Auras, L.-T. Lim, S. E. M. Selke and H. Tsuji, *Poly(Lactic Acid): Synthesis, Structures, Properties, Processing, and Applications*, 2010, DOI: **10.1002/9780470649848**.

39 E. A. Schmitt, D. R. Flanagan and R. J. Linhardt, Importance of Distinct Water Environments in the Hydrolysis of Poly(Dl-Lactide-Co-Glycolide), *Macromolecules*, 1994, **27**(3), 743–748, DOI: **10.1021/ma00081a019**.

40 H. K. Makadia and S. J. Siegel, Poly Lactic-Co-Glycolic Acid (PLGA) as Biodegradable Controlled Drug Delivery Carrier, *Polymers*, 2011, **3**(3), 1377–1397, DOI: **10.3390/polym3031377**.

41 F. Von Burkersroda, L. Schedl and A. Göpferich, Why Degradable Polymers Undergo Surface Erosion or Bulk Erosion, *Biomaterials*, 2002, **23**(21), 4221–4231, DOI: **10.1016/S0142-9612(02)00170-9**.

This journal is © The Royal Society of Chemistry 2025

J. Mater. Chem. B, 2025, **13**, 6376–6392 | **6391**

42 M.-N. Kim, B.-Y. Lee, I.-M. Lee, H.-S. Lee and J.-S. Yoon, Toxicity and Biodegradation of Products from Polyester Hydrolysis, *J. Environ. Sci. Health, Part A: Toxic/Hazard. Subst. Environ. Eng.*, 2001, **36**(4), 447–463, DOI: **10.1081/ESE-100103475**.

43 A. Verkhratsky, A. Butt, B. Li, P. Illes, R. Zorec, A. Semyanov, Y. Tang and M. V. Sofroniew, Astrocytes in Human Central Nervous System Diseases: A Frontier for New Therapies, *Signal Transduction Targeted Ther.*, 2023, **8**, 396, DOI: **10.1038/s41392-023-01628-9**.

44 J. McNeill, C. Rudyk, M. E. Hildebrand and N. Salmaso, Ion Channels and Electrophysiological Properties of Astrocytes: Implications for Emergent Stimulation Technologies, *Front. Cell. Neurosci.*, 2021, **15**, 644126, DOI: **10.3389/FNCEL.2021.644126/BIBTEX**.

45 M. Stepniewski, A. Bunker, M. Pasenkiewicz-Gierula, M. Karttunen and T. Róg, Effects of the Lipid Bilayer Phase State on the Water Membrane Interface, *J. Phys. Chem. B*, 2010, **114**(36), 11784–11792, DOI: **10.1021/jp104739a**.

46 M. Stepniewski, M. Pasenkiewicz-Gierula, T. Rog, R. Danne, A. Orlowski, M. Karttunen, A. Urtti, M. Yliperttula, E. Vuorimaa and A. Bunker, Study of PEGylated Lipid Layers as a Model for PEGylated Liposome Surfaces: Molecular Dynamics Simulation and Langmuir Monolayer Studies, *Langmuir*, 2011, **27**(12), 7788–7798, DOI: **10.1021/la200003n**.

47 A. Magarkar, E. Karakas, M. Stepniewski, T. Róg and A. Bunker, Molecular Dynamics Simulation of PEGylated Bilayer Interacting with Salt Ions: A Model of the Liposome Surface in the Bloodstream, *J. Phys. Chem. B*, 2012, **116**(14), 4212–4219, DOI: **10.1021/jp300184z**.

48 S. Rissanen, M. Kumorek, H. Martinez-Seara, Y.-C. Li, D. Jamróz, A. Bunker, M. Nowakowska, I. Vattulainen, M. Kepczynski and T. Róg, Effect of PEGylation on Drug Entry into Lipid Bilayer, *J. Phys. Chem. B*, 2014, **118**(1), 144–151, DOI: **10.1021/jp4105745**.

49 M. Lampin, R. Warocquier-Clérout, C. Legris, M. Degrange and M. F. Sigot-Luizard, Correlation between Substratum Roughness and Wettability, Cell Adhesion, and Cell Migration, *J. Biomed. Mater. Res.*, 1997, **36**(1), 99–108, DOI: **10.1002/(SICI)1097-4636(199707)36:1<99::AID-JBM12>3.0.CO;2-E**.

50 M. J. P. Biggs, R. G. Richards and M. J. Dalby, Nanotopographical Modification: A Regulator of Cellular Function through Focal Adhesions, *Nanomedicine*, 2010, **6**(5), 619–633, DOI: **10.1016/j.nano.2010.01.009**.

51 T.-W. Chung, D.-Z. Liu, S.-Y. Wang and S.-S. Wang, Enhancement of the Growth of Human Endothelial Cells by Surface Roughness at Nanometer Scale, *Biomaterials*, 2003, **24**(25), 4655–4661, DOI: **10.1016/S0142-9612(03)00361-2**.

52 D. Ganguly, C. D. L. Johnson, M. K. Gottipati, D. Rende, D.-A. Borca-Tasciuc and R. J. Gilbert, Specific Nanoporous Geometries on Anodized Alumina Surfaces Influence Astrocyte Adhesion and Glial Fibrillary Acidic Protein Immunoreactivity Levels, *ACS Biomater. Sci. Eng.*, 2018, **4**(1), 128–141, DOI: **10.1021/acsbiomaterials.7b00760**.

53 K. K. Elineni and N. D. Gallant, Regulation of Cell Adhesion Strength by Peripheral Focal Adhesion Distribution, *Biophys. J.*, 2011, **101**(12), 2903–2911, DOI: **10.1016/j.bpj.2011.11.013**.

54 C. Selhuber-Unkel, T. Erdmann, M. López-García, H. Kessler, U. S. Schwarz and J. P. Spatz, Cell Adhesion Strength Is Controlled by Intermolecular Spacing of Adhesion Receptors, *Biophys. J.*, 2010, **98**(4), 543–551, DOI: **10.1016/j.bpj.2009.11.001**.

55 C. Galli, L. Parisi, L. Elviri, A. Bianchera, A. Smerieri, P. Lagonegro, S. Lumetti, E. Manfredi, R. Bettini and G. M. Macaluso, Chitosan Scaffold Modified with D-(+) Raffinose and Enriched with Thiol-Modified Gelatin for Improved Osteoblast Adhesion, *Biomed. Mater.*, 2016, **11**(1), 015004, DOI: **10.1088/1748-6041/11/1/015004**.

56 E. A. Mun, A. C. Williams and V. V. Khutoryanskiy, Adhesion of Thiolated Silica Nanoparticles to Urinary Bladder Mucosa: Effects of PEGylation, Thiol Content and Particle Size, *Int. J. Pharm.*, 2016, **512**(1), 32–38, DOI: **10.1016/j.ijpharm.2016.08.026**.

57 O. Hegedus, D. Juriga, E. Sipos, C. Voniatis, A. Juhász, A. Idrissi, M. Zrínyi, G. Varga, A. Jedlovszky-Hajdú and K. S. Nagy, Free Thiol Groups on Poly(Aspartamide) Based Hydrogels Facilitate Tooth-Derived Progenitor Cell Proliferation and Differentiation, *PLoS One*, 2019, **14**(12), e0226363, DOI: **10.1371/journal.pone.0226363**.

58 L. J. Dooling, M. E. Buck, W. B. Zhang and D. A. Tirrell, Programming Molecular Association and Viscoelastic Behavior in Protein Networks, *Adv. Mater.*, 2016, **28**(23), 4651–4657, DOI: **10.1002/adma.201506216**.

59 E. Brotfain, S. E. Gruenbaum, M. Boyko, R. Kutz, A. Zlotnik and M. Klein, Neuroprotection by Estrogen and Progesterone in Traumatic Brain Injury and Spinal Cord Injury, *Curr. Neuropharmacol.*, 2016, **14**(6), 641–653, DOI: **10.2174/1570159X14666160309123554**.

60 W. C. Oliver and G. M. Pharr, Improved Technique for Determining Hardness and Elastic Modulus Using Load and Displacement Sensing Indentation Experiments, *J. Mater. Res.*, 1992, **7**(6), 1564–1580.

61 T.-H. Fang and W.-J. Chang, Nanoindentation Characteristics on Polycarbonate Polymer Film, *Microelectron. J.*, 2004, **35**(7), 595–599, DOI: **10.1016/j.mejo.2004.02.004**.

6392 | *J. Mater. Chem. B*, 2025, **13**, 6376–6392

This journal is © The Royal Society of Chemistry 2025